Atmospheric
Chemistry
and Physics
Discussions

1 Variations and sources of volatile organic compounds (VOCs)

2 in urban region: insights from measurements on a tall tower

3 Xiao-Bing Li[1,2], Bin Yuan[1,2,*], Sihang Wang[1,2], Chunlin Wang[3,4], Jing Lan[3,4], Zhijie

4 Liu[1,2], Yongxin Song[1,2], Xianjun He[1,2], Yibo Huangfu[1,2], Chenglei Pei[5,6,7,8], Peng

5 Cheng[9], Suxia Yang[1,2], Jipeng Qi[1,2], Caihong Wu[1,2], Shan Huang[1,2], Yingchang You[1,2],

6 Ming Chang[1,2], Huadan Zheng[10], Wenda Yang[9], Xuemei Wang[1,2], and Min Shao[1,2]

7 [1] Institute for Environmental and Climate Research, Jinan University, Guangzhou

8 511443, China

9 [2] Guangdong-Hongkong-Macau Joint Laboratory of Collaborative Innovation for

10 Environmental Quality, Guangzhou 511443, China

11 [3] Guangzhou Climate and Agrometeorology Center, Guangzhou, 511430, China

12 [4] Southern Marine Science and Engineering Guangdong Laboratory (Zhuhai), Zhuhai,

13 519082, China

14 [5] State Key Laboratory of Organic Geochemistry and Guangdong Key Laboratory of

15 Environmental Protection and Resources Utilization, Guangzhou Institute of

16 Geochemistry, Chinese Academy of Sciences, Guangzhou 510640, China

17 [6] CAS Center for Excellence in Deep Earth Science, Guangzhou, 510640, China

18 [7] University of Chinese Academy of Sciences, Beijing 100049, China

19 [8] Guangzhou Ecological and Environmental Monitoring Center of Guangdong Province,

20 Guangzhou 510060, China

21 [9] Institute of Mass Spectrometer and Atmospheric Environment, Jinan University,

22 Guangzhou 510632, Guangdong, China

23 [10] Guangdong Provincial Key Laboratory of Optical Fiber Sensing and

24 Communications, and Department of Optoelectronic Engineering, Jinan University,

25 Guangzhou, 510632, China

26 [*] Corresponding authors: byuan@jnu.edu.cn

Abstract

Volatile organic compounds (VOCs) are key precursors of ozone and particulate matter that are the two dominant air pollutants in urban environments. However, compositions and sources of VOCs in urban air aloft were rarely reported by far. To address this matter, highly time-resolved measurements of VOCs were made by proton-transfer-reaction time-of-flight mass spectrometer (PTR-ToF-MS) at a 450-m platform on the Canton Tower in Guangzhou, China. A combination of *in-situ* measurements and modeling techniques was used to characterize variations and sources of VOCs. Five sources were identified from positive matrix factorization (PMF) analysis, namely daytime-mixed (e.g., biogenic emissions and secondary formation), visitor-related (e.g., human breath and volatilization of ethanol-containing products), vehicular+industrial, regional transport, and volatile chemical product (VCP)-dominated (i.e., volatilization of personal care products), contributing on average to 22%, 30%, 28%, 10%, and 11% of total VOC (TVOC) mixing ratios, respectively. We observe that contributions of the visitor-related source, mainly composed of ethanol, followed well with the variation patterns of visitor number on the tower. The VCP-dominated source only had an average contribution of ~5.7 ppb during the campaign, accounting for a small fraction (11%) of TVOC mixing ratios. However, large fractions of some VOC species, e.g., monoterpenes (49%), were attributed to the VCP-dominated source, indicating significant contributions of VCPs to ambient concentrations of these species in urban environments. Vertical profiles of air pollutants (including NOx, ozone, Ox, and $PM_{2.5}$), measured at 5 m, 118 m, 168 m, and 488 m, exhibited more evident gradients at night than in the daytime owing to stronger stability of the nocturnal boundary layer. Mixing ratios of VOC species during the nighttime generally decreased with time when the 450-m platform was located in the nocturnal residual layer and significantly increased when impacted by emissions at ground. The results in this study demonstrated composition characteristics and sources of VOCs in urban air aloft, which could provide

54   valuable implications in making control strategies of VOCs and secondary air pollutants.

1 Introduction

Volatile organic compounds (VOCs) are important trace gases in the atmosphere and are composed of myriad chemical species (Pallavi et al., 2019; Wang et al., 2020a; Gkatzelis et al., 2021). Except for their direct adverse impacts on human health (Zhang et al., 2013), VOCs also contributed significantly to the formation of secondary pollutants such as ozone and secondary aerosol (Vo et al., 2018; Zhou et al., 2019; Qin et al., 2021). Reduction in ambient VOCs concentrations is the key for synergistic control of both ozone and particle pollution. However, it is highly challenging for this target due to complex sources and chemical transformations of VOCs in urban environments (Yuan et al., 2012; Mo et al., 2016; Zhu et al., 2019).

In addition to compiling accurate emission inventories (bottom-up method) (Zheng et al., 2013; An et al., 2021), the combination of *in-situ* measurements and receptor models (top-down method) was widely adopted to quantitatively apportion sources of ambient VOCs (Baudic et al., 2016; Liu et al., 2016; Fan et al., 2021; Pernov et al., 2021). Concentrations of various VOC species could be measured by offline and online techniques. Gas chromatography-flame ionization detector/mass spectrometry (GC-FID/MS) combined with stainless steel canisters were the most popular offline technique for VOCs measurements (Guo et al., 2011; Yuan et al., 2013; Zhang et al., 2013; Qin et al., 2021). Automated online GC-FID system and high time resolution mass spectrometer, such as proton-transfer-reaction mass spectrometer (PTR-MS) and chemical ionization mass spectrometer (CIMS), were popular online techniques for VOCs measurements (de Gouw and Warneke, 2007; Wang et al., 2020a; Wang et al., 2020c; Fan et al., 2021; Ye et al., 2021). However, VOCs measurements made by both online and offline instruments are significantly affected by very local emission sources, particularly in urban environments, when they are usually deployed at ground level. This is highly important for studies aiming to characterize variations and sources of ambient VOCs at large spatial scales (such as a city or city clusters) based on

Atmospheric
Chemistry
and Physics
Discussions
Open Access
EGU

82   measurements of only one site. To address this concern, VOCs measurements made in

83   the upper part of the planetary boundary layer (PBL) may be a better choice due to the

84   well mixing of surface emissions when being transported upward from sources to

85   observation sites (Hu et al., 2015a; Hu et al., 2015b; Squires et al., 2020).

86   As reported in the literature, *in-situ* measurements of VOCs at high altitudes (e.g.,

87   hundreds of meters or several kilometers above ground level) were predominantly made

88   using the combination of offline techniques and samples collected by various platforms

89   such as aircraft (Geng et al., 2009; Xue et al., 2011; Benish et al., 2020), tethered

90   balloons (Zhang et al., 2018; Wu et al., 2020b; Wang et al., 2021; Wu et al., 2021), high

91   buildings and towers (Ting et al., 2008; Mo et al., 2020), and unmanned aerial vehicles

92   (UAVs) (Vo et al., 2018; Liu et al., 2021). These offline measurements were

93   predominantly used to reveal vertical variations of VOCs concentrations, impacts of

94   VOCs degradation chemistry on the formation of secondary pollutants, and source

95   characteristics of the species of interest. Offline measurements made at high altitudes

96   were generally not capable of fully characterizing temporal variations of concentrations

97   and source characteristics of VOCs due to strict limitations in their time resolution and

98   sample sizes. In this condition, online VOCs measurements with fast response at high

99   altitudes are required. Lack of available platforms has been a key limited factor for

100   conducting online VOCs measurements at high altitudes in China. For instance, the

101   combined utilization of aircraft and online spectrometer (such as PTR-MS) has been

102   widely used in North America to measure VOCs concentrations in the lower

103   troposphere (Hornbrook et al., 2011; Müller et al., 2016; Yuan et al., 2016; Koss et al.,

104   2017; Fry et al., 2018; Chen et al., 2019), while it is quite difficult in China due to the

105   lack of professional research aircraft and the strict control of airspace. Tethered balloons

106   and UAVs are generally not suitable for online VOCs measurements due to their limited

107   payloads (Dieu Hien et al., 2019). Tower-based platforms provide another path for

108   online VOCs measurements at high altitudes in urban environments. However, tower-

109   based online measurements of VOCs were only reported in Beijing, China by far

110   (Squires et al., 2020; Zhang et al., 2020).

111   In this study, continuous online VOCs measurements, including more than 200

112   chemical species with a time resolution of 10 s, were made at a 450-m platform on the

113   Canton Tower in the Pearl River Delta (PRD) region, China during August–November

114   2020. A combination of the measurements and the positive matrix factorization (PMF)

115   receptor model was used to provide new insights into the concentrations, temporal

116   variations, and source contributions of VOCs in urban region.

2   Methods and materials

2.1 Site description and field campaign

119   The PRD region is one of the most developed city clusters in China with more

120   than 70 million residents by 2020 and is suffering from air pollution problems (e.g.,

121   ozone and secondary aerosol) (Wang et al., 2017; Wang et al., 2020b; Yan et al., 2020;

122   Li et al., 2022). In this study, VOCs measurements were made at the Canton Tower

123   (CTT, 23.11°N, 113.33°E) in Guangzhou, a large city in PRD (Figure S1), from August

124   18 to November 5 in 2020. The CTT has a total height of 610 m including the shaft on

125   the top. The observation was conducted in a room (Figure S1) at the 450-m Look Out

126   platform (Jin et al., 2022). The 450-m Look Out platform is a famous tourist attraction

127   with an opening time of local time (LT, UTC+8) 10:00–22:30, and visitors could walk

128   around for a panorama of downtown Guangzhou. On each day, there are two busiest

129   tourist hours, roughly at LT 11:00-14:00 and 18:00-21:00, on the 450-m platform. In

130   addition, there are three restaurants between 376 and 423 m. The VOCs measurements

131   were interrupted during October 8–12 due to instrument malfunction.

2.2 VOCs measurements

133   VOCs measurements were made using a high-resolution proton-transfer-reaction

134   quadrupole interface time-of-flight mass spectrometer (PTR-QiToF-MS, Ionicon

135   Analytik, Innsbruck, Austria) with both hydronium ion (H_3O^+) and nitric oxide ion

136   (NO^+) chemistry (Yuan et al., 2017; Wang et al., 2020a; Wu et al., 2020a). The H_3O^+

137   and NO^+ modes were automatically switched with 22 min for the H_3O^+ mode and 12

138   min for the NO^+ mode during the campaign. In this study, only VOCs measurements

139   made in the H_3O^+ mode were used for analysis. The sampling inlet of the instrument

140   was extended to the outside wall of the observation room using a ~5-m long

141   Perfluoroalkoxy (PFA) Teflon tubing (OD: 1/4"), which is drawn by a pump at a flow

142   rate of ~5 L min^{-1}. Blank measurements were performed automatically at the last 2 min

143   of the H_3O^+ mode by passing ambient air through a platinum catalyst heated to 365 ℃.

144   Mass spectra of up to m/z = 510 were obtained at a time resolution of 10 s.

145   A gas standard with 35 VOC species (Table S1) was used for calibrations of the

146   PTR-ToF-MS once per day. Ten organic acids and nitrogen-containing VOC species

147   were calibrated using a liquid calibration unit in the laboratory (Table S1). Sensitivities

148   of the remaining VOC species were determined using the quantification method based

149   on reaction kinetics of the PTR-ToF-MS (Wu et al., 2020a; He et al., 2022). Impacts of

150   the change in ambient humidity on measured signals of the PTR-ToF-MS were removed

151   using humidity-dependence curves of VOC species determined in the laboratory (Wang

152   et al., 2020a; Wu et al., 2020a). The limit of detection (LOD) for a VOC species was

153   defined as the concentration when the signal-to-noise ratio (SNR) equals to 3 (Yuan et

154   al., 2017). Average mixing ratios, LOD, sensitivities, chemical formula, and suggested

155   compounds of 225 VOC species used in this study are summarized in Table S1.

156   **2.3 Other measurements**

157   During the CTT campaign, a CO_2 and H_2O Gas Analyzer (Model: Li-840A, Licor

158   Inc., USA) was deployed to measure carbon dioxide (CO_2, ppm) and humidity (mmol

159   mol^{-1}). In addition, four air quality automatic monitoring stations are located at ground

160   level (~5 m), 118 m, 168 m, and 488 m of the tower, which report hourly concentrations

161   of O_3, NO, NO_2, NOx, and $PM_{2.5}$ along with meteorological parameters including

162   temperature (T), relatively humidity (RH), and pressure (Mo et al., 2020). Mass

163   concentrations of gaseous pollutants were reported at 25 ℃ and 1013.25 hPa and were

Atmospheric
Chemistry
and Physics
Discussions
Open Access
EGU

164   converted to mixing ratios (ppb) accordingly. A ceilometer (CL31, Vaisala, Finland)

165   deployed on the Panyu Campus of Jinan University (23.02°N, 113.41°E, Figure S1),

166   approximately 13.5 km to the southeast of the CTT, was used to measure planetary

167   boundary layer height (PBLH) during the camapign. In addition, measurements of

168   VOCs and CO_2 made on the campus of Guangzhou Institute of Geochemistry (GIG),

169   Chinese Academy of Sciences (23.15°N, 113.36°E, ~25 m above ground level) during

170   September–November 2018 (Wang et al., 2020a; Wang et al., 2020c; Wu et al., 2020a)

171   were used for comparison with those measured on the CTT. The GIG site is located

172   approximately 5.7 km to the northeast of the CTT. Measurements of VOCs and CO_2 at

173   the GIG site were made using the same instruments as those at the CTT site.

2.4 PMF receptor model

175   The PMF receptor model was used to quantitatively analyze sources of the VOC

176   measurements made at the 450-m platform. The PMF model has been widely used to

177   determine source contributions of measured VOCs concentrations in previous studies

178   (Yuan et al., 2012; Pallavi et al., 2019; Pernov et al., 2021). A simple description of the

179   PMF model was provided in the Supplementary Information (SI).

180   The PMF model was performed on 225 VOC species in this study (Table S1). In

181   preparation of PMF input data, measured concentrations of a VOC species below the

182   LOD were replaced with half of the LOD and corresponding uncertainties were

183   assigned to 5/6 of the LOD. Missing samples of a VOC species were replaced with its

184   median value during the campaign and corresponding uncertainties were set as values

185   equal to three times the median value (Zhang et al., 2013; Pernov et al., 2021; Qin et

186   al., 2021). In this study, the measured ethanol concentrations on the 450-m platform

187   were significantly impacted by the change in the number of visitors (a detailed

188   discussion in Section 3.3) and exhibited strong variations during the campaign (Figure

189   1). Thus, measurement uncertainties of ethanol calculated by Eq. (S3) were reduced by

190   a factor of 5 to increase the weight of ethanol in PMF analysis, which successfully

191   resolved factors representing visitor influences and significantly reduce residuals of

192   PMF solution from over 20% to ~14%. The PMF analysis was performed using the

193   PMF Evaluation Tool (v3.05) with Igor Pro (Ulbrich et al., 2009).

3   Results and discussion

3.1   Overview of field measurements during the campaign

196   As shown in Figure 1, concentrations of various species and meteorological

197   parameters all exhibited strong variations during the campaign. Daily mean ozone

198   mixing ratios varied in the range of 17.8–105.0 ppb with an average (± standard

199   deviation) of 55.1 ± 18.3 ppb. Daily mean total VOC (TVOC) mixing ratios, including

200   a total of 225 species, varied between 23.9–124.2 ppb with an average of 62.1 ± 21.8

201   ppb. Daily mean NOx mixing ratios varied in the range of 7.9–31.6 ppb with an average

202   of 13.6 ± 3.8 ppb. Measured CO_2 mixing ratios exhibited strong variability with daily

203   mean values ranging from 403.5 to 471.4 ppm. Ethanol was the most abundant VOC

204   species, accounting on average for 23.5% of measured TVOC mixing ratios during the

205   campaign. Daily mean ethanol mixing ratios varied between 4.3–53.4 ppb with an

206   average of 15.3 ± 9.1 ppb. Toluene was the most abundant aromatic species and had an

207   average mixing ratio of 1.4 ± 0.9 ppb during the campaign. Daily mean temperatures

208   varied in the range of 17.7–29.0 ℃ with an average of 23.2 ± 3.0 ℃. Daily mean RH

209   varied between 39.3%–85.0% with an average of $71.6\% \pm 10.3\%$. In general, the

210   observation site was predominantly influenced by hot and moist air masses from August

211   18 to October 4, but cooler and dryer air masses from October 5 to November 5.

212   The most abundant 10 VOC species measured by PTR-ToF-MS during the

213   campaign were ethanol, methanol, acetic acid, formaldehyde, acetone, ethyl acetate,

214   acetaldehyde, hydroxyacetone+propionic acid, toluene, and C8 aromatics, contributing

215   to over 70% of TVOC mixing ratios. As shown in Figure 2, the 225 VOC species were

216   classified into six categories, namely C_xH_y (i.e., hydrocarbons), $C_xH_yO_1$ (i.e., VOC

217   species containing one oxygen atom), $C_xH_yO_2$ (i.e., VOC species containing two

218   oxygen atoms), $C_xH_yO_{\geq 3}$ (i.e., VOC species containing more than three oxygen atoms),

219   N/S containing species (i.e., VOC species containing nitrogen or sulfur atoms), and

220   siloxanes (Wu et al., 2020a; He et al., 2022). The most abundant category was $C_xH_yO_1$,

221   which had an average contribution of 62.2% to measured TVOC mixing ratios. The

222   $C_xH_yO_2$ and $C_xH_yO_{\geq 3}$ categories contributed to 24.9% and 2.9% of measured TVOC

223   mixing ratios, respectively. C_xH_y was the third abundant category, accounting for 6.4%

224   of measured TVOC mixing ratios. Concentrations of N/S containing species and

225   siloxanes were generally lower than 0.5 ppb and only contributed to 1.3% and 2.4% of

226   measured TVOC mixing ratios, respectively.

227   As shown in Figure 2, the majority of the C_xH_y, $C_xH_yO_3$, and N/S containing

228   species measured at 450 m (CTT campaign) had lower mixing ratios than those

229   measured at ground level (GIG campaign), indicating their predominant contributions

230   from surface emission sources. Most of the $C_xH_yO_1$ and $C_xH_yO_2$ species measured at

231   450 m had comparable mixing ratios to those measured at the ground level. However,

232   mixing ratios of some $C_xH_yO_2$, $C_xH_yO_3$, and N/S containing species measured at 450 m

233   were significantly higher than at the ground level, which can be attributable to either

234   enhancement of their emissions on the 450-m platform or more secondary formation

235   from oxidation of VOCs (e.g., C_xH_y and $C_xH_yO_1$ species).

3.2   Diurnal variations in selected VOC species

237   Average diurnal profiles of nine selected VOC species measured by PTR-ToF-MS

238   during the campaign are demonstrated in Figure 3. Measurement results at GIG in 2018

239   are also shown for comparison to investigate differences in their diurnal variation

240   patterns and likely sources when measured at ground level and in urban upper air. In

241   addition, average diurnal profiles of the selected VOC species on working and non-

242   working days (including weekends and public holidays when the 450-m platform had

243   more visitors) during the CTT campaign are compared to explore potential emissions

244   from visitors. Meteorological factors including temperature and RH exhibited

245   insignificant differences between working and non-working days (Figure S2). Thus,

246   differences of concentrations between working and non-working days for various

Atmospheric
Chemistry
and Physics
Discussions

Open Access

EGU

247   species were not caused by the change in meteorological conditions.

248   Diurnal profiles of aromatic species, including benzene, toluene, and C8 aromatics

249   measured at 450 m exhibited similar variability with minima occurring between LT

250   12:00–16:00. Aromatics with higher chemical reactivity could be removed more rapidly

251   by reactions with hydroxyl radicals (OH) in the daytime (Yuan et al., 2012; Wu et al.,

252   2020a). In addition, significant elevation of daytime PBL could enhance the dilution of

253   chemical species, leading to rapid decreases in their concentrations (Sangiorgi et al.,

254   2011; Zhang et al., 2018). The two effects are the two most important factors for

255   controlling diurnal profiles of aromatics measured at 450 m. By contrast, diurnal

256   profiles of aromatics measured at ground displayed a different pattern with two peaks

257   occurring in the morning (LT 07:00–08:00) and evening (LT 19:00–22:00), respectively.

258   Diurnal patterns of aromatics are highly consistent with that of NOx (a typical tracer of

259   traffic emissions in urban region) at the ground level but were significantly different

260   from that of NOx at 450 m (Figure 4). Therefore, measured concentrations of aromatics,

261   particularly for benzene, were significantly affected by traffic emissions at ground level,

262   but contributed by more complex sources at 450 m. The diurnal profiles of aromatics

263   on working and non-working days exhibited minor differences, implying insignificant

264   contributions from visitor-related emissions. On working days, toluene concentrations

265   measured at 450 m were more affected by traffic emissions as manifested by the two

266   significant peaks in the morning and late afternoon.

267   Isoprene and monoterpenes exhibited distinct diurnal variation patterns during the

268   two campaigns. As reported in (Gómez et al., 2020; Tan et al., 2021), diurnal profiles

269   of isoprene and monoterpenes concentrations in non-urban regions usually displayed

270   unimodal patterns with a peak occurring at noon due to the strong light/temperature-

271   dependence of biogenic emissions. In this study, isoprene concentrations at 450 m

272   plateaued during the daytime and were slightly higher on non-working days than those

273   on working days, implying significant contributions from visitor-related emissions. The

274   diurnal profile of monoterpenes measured at 450 m exhibited a bi-modal pattern with

275 two peaks at LT 14:00 and 20:00, which was roughly in accordance with diurnal peaks

276 of visitor numbers on the 450-m platform. In addition, monoterpenes concentrations at

277 450 m were significantly higher on non-working days (particularly during the busiest

278 tourist hours) than on working days, confirming significant contributions from visitor-

279 related or cooking emissions (Klein et al., 2016). The diurnal profiles of methyl vinyl

280 ketone (MVK) + methacrolein (MACR) demonstrated similar shapes to ozone at both

281 450 m and ground level with maxima occurring between LT 13:00–15:00 (Figure 4),

282 consistent with MVK+MACR as photooxidation products of isoprene (Greenberg et al.,

283 1999; Zhao et al., 2021). The concentrations of MVK+MACR during the daytime on

284 non-working days were also evidently higher than those on working days, which are

285 consistent with isoprene observations.

286   Acetone, methanol, and ethanol are abundant OVOC species in urban atmosphere.

287 Diurnal profiles of acetone measured at both 450 m and the ground level were

288 characterized by higher concentrations in the daytime, suggesting significant

289 contributions from daytime sources, such as vegetation emissions and photooxidation

290 of hydrocarbons (Hu et al., 2013; Gkatzelis et al., 2021). In addition, acetone

291 concentrations at 450 m were higher on non-working days than on working days,

292 implying prominent contributions from visitor-related emissions. Diurnal profiles of

293 methanol and ethanol measured at ground level were characterized by a bimodal pattern

294 with two peaks occurring in the morning (LT 08:00) and evening (LT 20:00),

295 respectively, confirming significant contributions from traffic emissions. However,

296 methanol concentrations measured at 450 m exhibited insignificant diurnal variability

297 and lower concentrations on non-working days, indicating that they were less affected

298 by visitor-related emissions. The diurnal profile of ethanol at 450 m displayed two

299 peaks at LT 13:00 and 19:00, respectively, which was in accordance with the two busiest

300 tourist hours of the 450-m platform. In addition, ethanol concentrations at 450 m on

301 non-working days were significantly higher than those on working days, particularly in

302 the opening hours of the 450-m platform. These results suggest that the ethanol

Atmospheric
Chemistry
and Physics
Discussions

Open Access

EGU

303   concentrations measured at 450 m were largely contributed by visitor-related emissions.

304   To further explore spatial scales of emission source regions for different VOC

305   species, autocorrelation profiles of their time series were calculated by offsetting time

306   from -120 to 120 min. As indicated in previous studies (Hayes et al., 2013; Hu et al.,

307   2016), species more affected by local sources would have a narrower autocorrelation

308   profile. As shown in Figure 4, peak widths of autocorrelation profiles for different

309   chemical species at 450 m varied significantly. Autocorrelation profiles of

310   monoterpenes, toluene, ethanol, methanol, and isoprene were relatively narrower (even

311   narrower than the autocorrelation profile of NOx), and thus sources of these species

312   had more local characteristics. Autocorrelation profiles of benzene, C8 aromatics,

313   acetone, and MVK+MACR were much flatter (but narrower than the autocorrelation

314   profile of ozone and Ox), indicating that concentrations of these species were more

315   contributed by sources at larger spatial scales. By contrast, peak widths of the

316   autocorrelation profiles for different chemical species (except for ethanol) varied

317   insignificantly at ground level and were similar to that of NOx. Therefore,

318   concentrations of the selected VOC species were significantly contributed by local

319   traffic emissions at ground level but contributed by more complex sources on larger

320   spatial scales at 450 m.

321   3.3   Impacts of visitor-related emissions on VOCs measurements

322   As introduced in section 2.1, the CTT campaign was conducted in August-

323   November of 2020, during which visitors were required to wear masks when visiting

324   the CTT and ethanol-containing products were widely used to prevent the spread of the

325   COVID-19 pandemic. For example, medicinal alcohol (75%) spray was widely used to

326   wipe public utilities and 75%-ethanol bacteriostatic gel was extensively used as

327   sanitizer for hands. Diurnal profiles of some VOC species (e.g., ethanol and

328   monoterpenes) exhibited similar diurnal patterns to the number of visitors at the 450-m

329   platform. Therefore, VOCs measurements made at the 450-m platform may be affected

330   by visitor-related emissions, such as human breath and evaporation of personal care

331 products (Veres et al., 2013).

332 As shown in Figure 5, the diurnal profile of CO_2 measured at 450 m increased

333 between LT 09:00–20:00, which was different from those measured at ground level.

334 The higher CO_2 mixing ratios at 450 m were predominantly contributed by human

335 breath due to the absence of combustion sources. Measured ethanol mixing ratios were

336 well correlated with those of CO_2 (r=0.62) during the CTT campaign, indicating that

337 ethanol concentrations, as well as its variations, were predominantly determined by the

338 change in the number of visitors on the tower. In addition, the CO_2 mixing ratios on

339 non-working days, especially during the busiest tourist hours, were markedly higher

340 than those on working days. As illustrated in Figure 5, the 450-m platform was closed

341 during October 13-15 as the result of the influence of Typhoon Kompasu. On these days,

342 mixing ratios of ethanol, CO_2, and monoterpenes exhibited similar variation patterns to

343 benzene (a typical tracer of traffic emissions). However, mixing ratios of ethanol, CO_2,

344 and monoterpenes exhibited quite different variation patterns from benzene when the

345 450-m platform was re-open (October 16–21). For instance, mixing ratios of ethanol,

346 CO_2, and monoterpenes generally decreased from LT 12:00 to 18:00 between October

347 13–15, but significantly increased during the same period between October 16–21.

348 Therefore, it can be concluded that the VOCs measurements made at the 450-m

349 platform were significantly affected by visitor-related emissions, which will be

350 quantitatively assessed using the PMF analysis in following sections.

3.4 Source analysis of VOCs measurements

352 In this study, a five-factor solution for the PMF analysis was chosen as the optimal

353 result. Figure 6 displays source profiles (m/z $\leq$ 150, the full range of the mass spectra

354 is shown in Figure S5) of the five PMF factors along with average diurnal profiles of

355 their contributions. The five factors were assigned to likely sources of daytime-mixed,

356 visitor-related, vehicular+industrial, regional transport, and volatile chemical product

357 (VCP)-dominated according to characteristics of their source profiles and temporal

358 variations, which are detailed discussed in the *SI*.

359   The visitor-related source predominantly includes contributions from human

360   breath and volatilization of personal care products. Contributions of the visitor-related

361   source had the narrowest autocorrelation profile among the five factors (Figure 6),

362   confirming its most local characteristics. As shown in Figure 7, the visitor-related

363   source had the largest contributions (15.9 ± 19.6 ppb), accounting for 30% of the

364   average TVOC mixing ratio. In addition, contributions of the visitor-related source

365   accounted for a larger fraction of TVOC mixing ratios on non-working days (33%) than

366   those on working days (28%). The vehicular+industrial source mainly includes

367   contributions from vehicular exhausts and emissions of various industrial processes.

368   Contributions of the vehicular+industrial source (15.1 ± 18.3 ppb) were comparable to

369   those of the visitor-related source, accounting for 28% of the average TVOC mixing

370   ratio. As also anticipated, the vehicular+industrial source contributed to a smaller

371   fraction of TVOC mixing ratios on non-working days (26%) than those on working

372   days (30%). The VCP-dominated source predominantly includes contributions from

373   VCPs in urban environments. The VCP-dominated source had an average contribution

374   of 5.7 ± 5.4 ppb, accounting for 11% of the average TVOC mixing ratio. The average

375   contribution of the VCP-dominated source in this study was comparable to those (~6.0

376   ppb) measured in New York City (Gkatzelis et al., 2021). However, VCPs contributed

377   to over 50% of anthropogenic VOCs emissions in New York City, which is significantly

378   greater than the fraction in this study (11%, and it will increase to 16% when

379   contributions of the visitor-related source were removed). In comparison to large cities

380   in U.S., traffic and industrial emissions were still dominant sources of ambient VOCs

381   in Chinese cities.

382   The daytime-mixed source predominantly includes contributions from biogenic

383   emissions and photooxidation products of various VOCs. As shown in Figure 7, the

384   daytime-mixed source had an average contribution of 11.6 ± 12.6 ppb, accounting for

385   21% of the average TVOC mixing ratio. It exhibited consistent diurnal variation

386   patterns on both working and non-working days but had larger contributions in the

387   daytime on non-working days (Figure 6). This may be attributed to the enhanced

388   formation of secondary OVOC species as manifested by the higher ozone

389   concentrations on non-working days (Figure S6). The regional transport source mainly

390   includes contributions from advection transport of aged air masses. Contributions of

391   the regional transport source had the flattest autocorrelation profile (Figure 6), implying

392   its most regional characteristics. Only a small fraction (<5%) of reactive chemical

393   species such as aromatics were attributed to this factor. Contributions of the regional

394   transport source accounted for 13% of the TVOC mixing ratio when affected by

395   continental airflows, but only accounted for 3% when affected by marine airflows

396   (Figure S7). By contrast, contributions of the other factors displayed insignificant

397   dependence on wind direction.

398   As shown in Figure 8, source apportionment of the selected VOC species (Figure

399   3) discussed in section 3.2 were further investigated. The vehicular+industrial source

400   had the largest contribution (36%) to benzene. The daytime-mixed source also

401   contributed to 18% of measured benzene mixing ratios. In addition, more than 20% of

402   benzene was attributed to the VCP-dominated source. In contrast to benzene, toluene

403   was predominantly attributed to the vehicular+industrial (93%) and visitor-related (7%)

404   sources. The average ratio of toluene to benzene was 5.7 ppb/ppb during the CTT

405   campaign (Figure S8), further confirming primary contributions of toluene from

406   vehicular and industrial emissions (Wu et al., 2016; Zhou et al., 2019; Xia et al., 2021).

407   The vehicular+industrial source also accounted for the largest fractions of C8 and C9

408   aromatics. In addition, 26% of C8 aromatics and 38% of C9 aromatics were attributed

409   to the VCP-dominated source. The other three sources in total contributed to less than

410   10% of concentrations of C8 and C9 aromatics. These results indicate that VCPs are

411   important sources of aromatics in urban environments but they were rarely identified

412   in previous studies.

413   Isoprene and monoterpenes are widely known tracers of biogenic emissions

414   (Millet et al., 2016; Zhao et al., 2021). However, the daytime-mixed source only

Atmospheric
Chemistry
and Physics
Discussions

Open Access

EGU

415 contributed to 16% of measured isoprene mixing ratios. By contrast, more than 70% of

416 isoprene were attributed to the visitor-related (38%) and VCP-dominated (35%) sources.

417 As for monoterpenes, more than 95% of the measured mixing ratios were attributed to

418 the visitor-related (47%) and VCP-dominated (49%) sources. The average ratio of

419 monoterpene to isoprene mixing ratios at 450 m was 0.84 in the daytime (LT 08:00–

420 18:00), which was significantly greater than that at the ground level (0.05) (Figure S8).

421 It further confirms significant contributions of monoterpenes from visitor-related

422 emissions at the 450-m platform. The daytime-mixed source did not exhibit discernible

423 contributions to monoterpenes. This agrees well with the results in New York City

424 where monoterpene mixing ratios were primarily attributed to anthropogenic sources

425 such as VCPs, cooking, and building materials (Coggon et al., 2021; Gkatzelis et al.,

426 2021). These results suggest that emission intensities of isoprene and monoterpenes

427 may be highly underestimated in urban regions if their anthropogenic emissions are

428 overlooked or less considered. This is exceedingly important for air quality models

429 when estimating formation of ozone and secondary organic aerosol driven by the

430 oxidation of isoprene and monoterpene. As the key photooxidation products of isoprene,

431 nearly 60% of MVK+MACR were attributed to the daytime-mixed source. The visitor-

432 related, regional transport, and VCP-dominated sources contributed to comparable

433 fractions (11%–15%) of MVK+MACR. Therefore, anthropogenic emissions are also

434 important sources of MVK+MACR in urban environments.

435 As shown in Figure 8, 39% of acetone was attributed to the daytime-mixed source.

436 The vehicular+industrial (19%) and VCP-dominated (21%) sources accounted for

437 comparable fractions of measured acetone mixing ratios. In addition, the visitor-related

438 source also contributed (7%) significantly to acetone. As for methanol, the

439 vehicular+industrial source accounted for the largest fraction (38%), followed by the

440 daytime-mixed (22%), regional transport (17%), VCP-dominated (14%), and visitor-

441 related (9%) sources. These results reveal that VCPs also contributed significantly to

442 ambient concentrations of acetone and methanol and should be carefully considered

443   when estimating their total emission intensities from anthropogenic sources. Ethanol

444   was predominantly attributed to the visitor-related source. Therefore, the enhanced

445   ethanol mixing ratios were not capable of representing its characteristic concentrations

446   in urban environments. Although the absence of synchronous ground-level

447   measurements, we can speculate that ethanol concentrations at ground level were also

448   significantly increased during the outbreak of the COVID-19 pandemic due to the

449   extensive usage of ethanol-containing products. The enhancement of ethanol

450   concentrations may contribute significantly to atmospheric OH reactivity (Millet et al.,

451   2012; de Gouw et al., 2017; de Gouw et al., 2018) and then regulate the formation of

452   secondary pollutants. Therefore, impacts of the ethanol enhancement on ambient air

453   quality should be explicitly investigated in future studies due to the wide report of ozone

454   enhancement during the outbreak of the COVID-19 pandemic (Huang et al., 2020; Qi

455   et al., 2021).

456   Acetonitrile is widely used as a typical tracer of biomass burning sources in

457   previous studies (de Gouw et al., 2003; Zhang et al., 2020; Tan et al., 2021). However,

458   biomass burning source was not identified in this study because acetonitrile was not

459   predominantly attributed to a single factor (Figure 8). In addition to the visitor-related

460   source, the other four sources also had significant contributions to acetonitrile. As

461   indicated by (Huangfu et al., 2021), it is not always suitable, particularly in urban

462   environments, to use absolute concentrations of acetonitrile as the indication of biomass

463   burning sources. The ratio of acetonitrile to CO is a better indicator to identify whether

464   VOC measurements are significantly contributed by biomass burning emissions. The

465   average ratio of acetonitrile to CO was only 0.09 (ppb ppm^{-1}) during the campaign

466   (Figure S8), indicating insignificant contributions from biomass burning sources. In

467   addition to the daytime-mixed (22%) and vehicular+industrial (26%) sources, the VCP-

468   dominated source (31%) was also an important source of acetonitrile in urban

469   environments.

3.5 Vertical distributions of air pollutants concentrations

470

471 As introduced in section 2.1, hourly concentrations of some air pollutants were

472 routinely measured at four automatic sites on the CTT. Figure 9 shows time series of

473 vertical profiles of NOx, ozone, Ox (O_3+NO_2), and $PM_{2.5}$ concentrations in September

474 2020. Concentrations of the four pollutants all exhibited significantly stratified

475 structures between 488 m and the ground level. Higher mixing ratios of ozone and Ox

476 predominantly occurred at higher altitudes, while higher NOx mixing ratios mainly

477 occurred at ground level. By contrast, higher $PM_{2.5}$ concentrations were observed at

478 both middle altitudes and ground level.

479 To further clarify vertical distribution patterns of air pollutants concentrations,

480 their composite profiles for daytime (LT 08:00–18:00), nighttime (LT 19:00–05:00),

481 and the whole day in the campaign were determined, respectively, as shown in Figure

482 10. Vertical profiles of air pollutants concentrations exhibited similar shapes both in

483 daytime and nighttime. NOx mixing ratios decreased from the ground level to 488 m,

484 suggesting intensive surface emissions around the CTT. Ozone mixing ratios rapidly

485 increased from the ground level to 488 m, which was consistent with the results reported

486 in previous studies (Velasco et al., 2008; Li et al., 2018; Zhang et al., 2019; Li et al.,

487 2021b). The positive gradients of ozone profiles are mainly caused by enhanced NO

488 titration (NO+O_3=O_2+NO_2) and dry deposition near ground. Ox mixing ratios also

489 increased from the ground level to 488 m but exhibited weaker gradients in comparison

490 to ozone. Vertical profiles of $PM_{2.5}$ concentrations exhibited similar shapes to NOx

491 during the campaign. Daily mean concentrations of $PM_{2.5}$ and Ox were well correlated

492 at the four altitudes with r values varying in the range of 0.61–0.82, suggesting

493 prominent contributions of secondary formation to ambient PM concentrations.

494 Moreover, the correlation coefficients between Ox and $PM_{2.5}$ concentrations at 488 m

495 (0.82) were greater than those at ground level (0.78), as they were less affected by

496 nearby vehicular emissions. This is consistent with the work by (Yan et al., 2020), who

497 reported that secondary components contributed to ~80% of $PM_{2.5}$ concentrations in

498   PRD over the 2008–2019 period.

499   As shown in Figures 9 and 10, vertical profiles of air pollutants concentrations

500   exhibited weaker gradients in the daytime than in the nighttime. Therefore, the daytime

501   VOC chemistry may have minor differences between the ground level and the 450-m

502   site due to strong vertical mixing of chemical species in the planetary boundary layer

503   (PBLH>450 m, as shown in Figure S9). In the nighttime, the oxidative products (such

504   as organic nitrates and OVOCs) of unsaturated hydrocarbons, predominantly initiated

505   by nitrate radicals (NO_3) and ozone, are also important precursors of secondary aerosol

506   (Warneke et al., 2004; Brown et al., 2011; Ng et al., 2017; Liebmann et al., 2019).

507   However, it is highly challenging to investigate the nighttime VOC chemistry with only

508   ground-level measurements due to the rapid removal of NO_3 radicals and ozone by

509   enhanced NO titration in the near-surface atmosphere (Geyer and Stutz, 2004; Stutz et

510   al., 2004; Brown et al., 2007). In this condition, the nocturnal residual layer, separated

511   from nocturnal boundary layer and remained, to a large extent, the chemical

512   composition of the daytime atmosphere, could provide an ideal place for investigating

513   nighttime VOC chemistry. Oxidative products of VOCs in the residual layer could be

514   mixed downward with the expansion of the PBL during the daytime (Geyer and Stutz,

515   2004; Stutz et al., 2004; Li et al., 2021a), contributing to the formation of ozone and

516   secondary aerosol at ground level. Investigation of the nighttime VOC chemistry was

517   one of the initial purposes of this study. Unfortunately, the 450-m site was rarely located

518   in the nocturnal residual layer during the campaign due to frequent occurrences of

519   cloudy and rainy weather. The average nighttime PBLH in Guangzhou was

520   approximately stabilized at 500 m during the campaign (Figure S9), implying

521   significant impacts from surface emissions on the measurements made at 450 m.

522   In addition to the measured PBLH data, formation of the residual layer at 450 m

523   could be also identified by comparing differences of ozone mixing ratios between 488

524   m and the ground level. Without fresh NO emissions, ozone mixing ratios in the

525   nocturnal residual layer were markedly higher than at ground level and exhibited

526   insignificant variability throughout the nighttime (Caputi et al., 2019; Udina et al.,

527   2020). By contrast, surface ozone mixing ratios are generally very low (close to zero)

528   due to enhanced titration by freshly emitted NO and strong inhibition of atmospheric

529   vertical mixing (Ma et al., 2011; Chen et al., 2020). In this study, the data collected

530   between September 27–30 was one of the cases discussed above and was used to briefly

531   describe behaviors of some representative VOC species (including ethanol,

532   monoterpene, styrene, phenol, and toluene) at 450 m.

533   As shown in Figure 11, ozone mixing ratios measured at ground level (10.2 ± 10.4

534   ppb) were significantly lower than those at 488 m (44.2 ± 19.6 ppb) on the nighttime

535   of September 27–30, indicating formation of the nocturnal residual layer lower than

536   450 m. On the nighttime of September 27–28, ozone mixing ratios at 488 m slightly

537   fluctuated around 46.8 ppb between LT 19:00–00:00 and suddenly decreased to 28.4

538   ppb at LT 01:00 on September 28. The sudden decrease in ozone at 488 m at LT 01:00

539   was accompanied by slight increases in both NOx and VOCs but significant decreases

540   in NOx and NO at ground level, indicating a transitory intrusion of surface fresh

541   emissions into the residual layer. On September 28, ozone mixing ratios at 488 m

542   slightly decreased from 33.0 to 31.5 ppb from LT 02:00 to 05:00, during which mixing

543   ratios of NOx and VOCs all decreased in different degrees. The continuous decreases

544   in both toluene and ethanol between LT 02:00–05:00 confirm that the VOCs

545   measurements at 450 m were free of interferences by fresh emissions due to their

546   significant contributions from vehicular exhausts (Figure 7). Toluene mixing ratios

547   decreased by 43% from LT 02:00 to 05:00, which was significantly larger than those

548   (12–27%) of the other VOC species shown in Figure 11. However, the NO3 reactivity

549   (characterized by reaction rate constants of VOC species to NO3 radical, k_{NO3}) of

550   toluene ($k_{NO3} = 7 \times 10^{-17}$ cm^{-3} molecule^{-1} s^{-1}) is exceedingly lower than those of the other

551   unsaturated VOC species (k_{NO3} varies in the magnitudes of 10^{-12} cm^{-3} molecule^{-1} s^{-1})

552   (Atkinson and Arey, 2003; Atkinson et al., 2006). Therefore, the decline of unsaturated

553   VOC species in the nocturnal residual layer may not be all attributed to the degradation

554   chemistry initiated by NO_3 radicals or ozone.

555   On the nighttime of September 28–29, the PBLH was higher than 500 m between

556   LT 19:00–00:00, resulting in significant decreases in ozone and increases in NOx and

557   VOCs. As shown in Figure 11, the 450-m site may locate in the residual layer after LT

558   01:00. However, the rapid decrease in mixing ratios of NOx and VOCs between LT

559   01:00–05:00 were not likely caused by chemical removal due to the rapid increase in

560   ozone. Regional transport of aged air masses (characterized by high ozone and low NOx

561   mixing ratios) may be responsible for the rapid decline in various VOC species in the

562   early morning of September 29. On the nighttime of September 29–30, the 450-m site

563   may be significantly impacted by surface fresh emissions as mixing ratios of ozone,

564   NOx, and VOCs all decreased between LT 19:00–01:00 and simultaneously increased

565   between LT 02:00–05:00. NOx and toluene mixing ratios generally increased between

566   LT 12:00–18:00 during September 27–29, which were quite different from their

567   average diurnal variation patterns during the whole campaign (Figures 3 and 4). As

568   discussed above, the 450-m site was located in the nocturnal residual layer during

569   September 27–29. Therefore, emissions of pollutants from surface sources could be

570   mixed upward to the measurement site only when the PBLH was higher than 450 m.

571   Furthermore, the PBL was relatively lower and rapidly shrank in the afternoon, leading

572   to the accumulation of chemical species at 450 m.

573   In summary, the VOCs measurements made by PTR-ToF-MS at the 450-m site

574   could be used to characterize variations in VOC species from their primary emissions

575   during the nighttime. Nevertheless, the oxidative degradation processes of VOCs in the

576   nighttime were not well captured. It is highly difficult to provide more information on

577   the nighttime chemistry of VOC species solely depending on their temporal variations.

578   We believe that the oxidative degradation of reactive VOC species did occur in the

579   nocturnal residual layer due to the coexistence of high concentrations of NOx and ozone.

580   Measurement techniques that targeting oxidation products (e.g., ToF-CIMS) and

581   numerical models should be jointly used to deeply analyze the nighttime chemistry of

582 VOCs in the nocturnal residual layer and quantitatively evaluate their impacts on

583 ambient air quality during the daytime.

4 Conclusions

585 Continuous measurements of VOCs mixing ratios were made by PTR-ToF-MS at

586 450 m on the CTT in PRD, China from August 18–November 5, 2020. In addition to

587 some specific VOC species (such as ethanol and monoterpenes) that were intensively

588 emitted by visitor-related sources, mixing ratios of most VOC species at 450 m were

589 generally lower than those at ground level. Due to intensive emissions from visitor-

590 related sources, mixing ratios of some VOC species were significantly higher on non-

591 working days than those on working days. The VOCs mixing ratios measured at 450 m

592 also exhibited different diurnal variations from those at ground level, indicating that

593 they were contributed by more mixed sources at larger spatial scales. Five sources,

594 namely daytime-mixed, visitor-related, vehicular+industrial, regional transport, and

595 VCP-dominated, were determined by the PMF model, contributing to 22%, 30%, 28%,

596 10%, and 11% of the average TVOC mixing ratio, respectively. In addition to the

597 daytime-mixed and visitor-related sources, the other three sources all had relatively

598 lower contributions on non-working days than on working days. The VCP-dominated

599 source contributed an average of 5.7 ppb to TVOC mixing ratios, which was

600 comparable to those reported in American cities (Gkatzelis et al., 2021). However, the

601 VCP-dominated source accounted for a much smaller fraction (11%) of measured

602 TVOC mixing ratios in this study than in U.S. cities (>50%). Therefore, the reduction

603 in anthropogenic VOC emissions from traffic and industrial sources are still priorities

604 of current air pollution control for Chinese cities. However, though smaller fraction of

605 VOCs contributed by VCPs was observed in this study compared to cities in U.S.

606 (McDonald et al., 2018; Gkatzelis et al., 2021), large fractions of key VOC species

607 (such as monoterpenes and some aromatic species) were attributed to the VCP-

608 dominated source. This may be important for formulating control strategies for specific

609 chemical species or when they are used as key tracers of certain emission sources.

610 The vertical distribution patterns of NOx, ozone, Ox, and $PM_{2.5}$ concentrations

611 were investigated using measurements made at four different heights on the CTT.

612 Vertical profiles of NOx and $PM_{2.5}$ generally exhibited negative gradients, while

613 vertical profiles of ozone generally demonstrated positive gradients. In addition, the

614 vertical gradients of air pollutants concentrations were larger in the nighttime than in

615 the daytime, predominantly owing to stronger stability of the nocturnal boundary layer.

616 The 450-m site was rarely located in the nocturnal residual layer as cloudy and rainy

617 weather dominated during the campaign. The selected case indicated that the NO_3- or

618 O_3-initiated degradation chemistry may be not the sole path for the removal of

619 unsaturated VOC species in the nocturnal residual layer. The degradation chemistry of

620 reactive VOC species in the nocturnal residual layer and their impacts on ground-level

621 air quality could be further investigated in combination with model simulations in

622 future studies.

Data availability

624 The observational data used in this study are available from corresponding authors upon

625 request.

Author contributions

627 XBL and BY designed the research. XBL, BY, SHW, CLW, JL, ZJL, XJH, YBHF, CLP,

628 CP, JPQ, CHW, YCY, MC, HDZ, WDY, XMW, and MS contributed to the data

629 collection and data analysis. XBL and BY performed the PMF analysis with

630 contributions from YXS, SXY, and SH. XBL and BY wrote the paper. All the coauthors

631 discussed the results and reviewed the paper.

Competing interests

633 The authors declare that they have no conflict of interest.

Atmospheric
Chemistry
and Physics
Discussions

Acknowledgments

References

644

645 An, J., Huang, Y., Huang, C., Wang, X., Yan, R., Wang, Q., Wang, H., Jing, S., Zhang,
646   Y., Liu, Y., Chen, Y., Xu, C., Qiao, L., Zhou, M., Zhu, S., Hu, Q., Lu, J., and Chen,
647   C.: Emission inventory of air pollutants and chemical speciation for specific
648   anthropogenic sources based on local measurements in the Yangtze River Delta
649   region, China, Atmos. Chem. Phys., 21, 2003-2025, https://doi.org/10.5194/acp-
650   21-2003-2021, 2021.
651 Atkinson, R., and Arey, J.: Atmospheric Degradation of Volatile Organic Compounds,
652   Chem Rev, 103, 4605-4638, https://doi.org/10.1021/cr0206420, 2003.
653 Atkinson, R., Baulch, D. L., Cox, R. A., Crowley, J. N., Hampson, R. F., Hynes, R. G.,
654   Jenkin, M. E., Rossi, M. J., Troe, J., and Subcommittee, I.: Evaluated kinetic and
655   photochemical data for atmospheric chemistry: Volume II – gas phase
656   reactions of organic species, Atmos. Chem. Phys., 6, 3625-4055,
657   https://doi.org/10.5194/acp-6-3625-2006, 2006.
658 Baudic, A., Gros, V., Sauvage, S., Locoge, N., Sanchez, O., Sarda-Estève, R.,
659   Kalogridis, C., Petit, J. E., Bonnaire, N., Baisnée, D., Favez, O., Albinet, A., Sciare,
660   J., and Bonsang, B.: Seasonal variability and source apportionment of volatile
661   organic compounds (VOCs) in the Paris megacity (France), Atmos. Chem. Phys.,
662   16, 11961-11989, https://doi.org/10.5194/acp-16-11961-2016, 2016.
663 Benish, S. E., He, H., Ren, X., Roberts, S. J., Salawitch, R. J., Li, Z., Wang, F., Wang,
664   Y., Zhang, F., Shao, M., Lu, S., and Dickerson, R. R.: Measurement report: Aircraft
665   observations of ozone, nitrogen oxides, and volatile organic compounds over
666   Hebei Province, China, Atmos. Chem. Phys., 20, 14523-14545,
667   https://doi.org/10.5194/acp-20-14523-2020, 2020.
668 Brown, S. S., Dubé, W. P., Osthoff, H. D., Stutz, J., Ryerson, T. B., Wollny, A. G., Brock,
669   C. A., Warneke, C., de Gouw, J. A., Atlas, E., Neuman, J. A., Holloway, J. S.,
670   Lerner, B. M., Williams, E. J., Kuster, W. C., Goldan, P. D., Angevine, W. M.,
671   Trainer, M., Fehsenfeld, F. C., and Ravishankara, A. R.: Vertical profiles in NO_3
672   and N_2O_5 measured from an aircraft: Results from the NOAA P-3 and surface
673   platforms during the New England Air Quality Study 2004, Journal of Geophysical
674   Research: Atmospheres, 112, https://doi.org/10.1029/2007JD008883, 2007.
675 Brown, S. S., Dubé, W. P., Peischl, J., Ryerson, T. B., Atlas, E., Warneke, C., de Gouw,
676   J. A., te Lintel Hekkert, S., Brock, C. A., Flocke, F., Trainer, M., Parrish, D. D.,
677   Feshenfeld, F. C., and Ravishankara, A. R.: Budgets for nocturnal VOC oxidation
678   by nitrate radicals aloft during the 2006 Texas Air Quality Study, Journal of
679   Geophysical Research: Atmospheres, 116, https://doi.org/10.1029/2011JD016544,
680   2011.
681 Caputi, D. J., Faloona, I., Trousdell, J., Smoot, J., Falk, N., and Conley, S.: Residual
682   layer ozone, mixing, and the nocturnal jet in California's San Joaquin Valley,
683   Atmos. Chem. Phys., 19, 4721-4740, https://doi.org/10.5194/acp-19-4721-2019,

684 2019.

685 Chen, Q., Li, X.-B., Song, R., Wang, H.-W., Li, B., He, H.-D., and Peng, Z.-R.:
686 Development and utilization of hexacopter unmanned aerial vehicle platform to
687 characterize vertical distribution of boundary layer ozone in wintertime,
688 Atmospheric Pollution Research, 11, 1073-1083,
689 https://doi.org/10.1016/j.apr.2020.04.002, 2020.

690 Chen, X., Millet, D. B., Singh, H. B., Wisthaler, A., Apel, E. C., Atlas, E. L., Blake, D.
691 R., Bourgeois, I., Brown, S. S., Crounse, J. D., de Gouw, J. A., Flocke, F. M., Fried,
692 A., Heikes, B. G., Hornbrook, R. S., Mikoviny, T., Min, K. E., Müller, M., Neuman,
693 J. A., O'Sullivan, D. W., Peischl, J., Pfister, G. G., Richter, D., Roberts, J. M.,
694 Ryerson, T. B., Shertz, S. R., Thompson, C. R., Treadaway, V., Veres, P. R., Walega,
695 J., Warneke, C., Washenfelder, R. A., Weibring, P., and Yuan, B.: On the sources
696 and sinks of atmospheric VOCs: an integrated analysis of recent aircraft
697 campaigns over North America, Atmos. Chem. Phys., 19, 9097-9123,
698 https://doi.org/10.5194/acp-19-9097-2019, 2019.

699 Coggon, M. M., Gkatzelis, G. I., McDonald, B. C., Gilman, J. B., Schwantes, R. H.,
700 Abuhassan, N., Aikin, K. C., Arend, M. F., Berkoff, T. A., Brown, S. S., Campos,
701 T. L., Dickerson, R. R., Gronoff, G., Hurley, J. F., Isaacman-VanWertz, G., Koss,
702 A. R., Li, M., McKeen, S. A., Moshary, F., Peischl, J., Pospisilova, V., Ren, X.,
703 Wilson, A., Wu, Y., Trainer, M., and Warneke, C.: Volatile chemical product
704 emissions enhance ozone and modulate urban chemistry, Proceedings of the
705 National Academy of Sciences, 118, e2026653118,
706 https://doi.org/10.1073/pnas.2026653118, 2021.

707 de Gouw, J., and Warneke, C.: Measurements of volatile organic compounds in the
708 earth's atmosphere using proton-transfer-reaction mass spectrometry, Mass
709 Spectrom Rev, 26, 223-257, https://doi.org/10.1002/mas.20119, 2007.

710 de Gouw, J. A., Warneke, C., Parrish, D. D., Holloway, J. S., Trainer, M., and Fehsenfeld,
711 F. C.: Emission sources and ocean uptake of acetonitrile (CH3CN) in the
712 atmosphere, Journal of Geophysical Research: Atmospheres, 108,
713 https://doi.org/10.1029/2002JD002897, 2003.

714 de Gouw, J. A., Gilman, J. B., Kim, S.-W., Lerner, B. M., Isaacman-VanWertz, G.,
715 McDonald, B. C., Warneke, C., Kuster, W. C., Lefer, B. L., Griffith, S. M.,
716 Dusanter, S., Stevens, P. S., and Stutz, J.: Chemistry of Volatile Organic
717 Compounds in the Los Angeles basin: Nighttime Removal of Alkenes and
718 Determination of Emission Ratios, Journal of Geophysical Research: Atmospheres,
719 122, 11,843-811,861, https://doi.org/10.1002/2017JD027459, 2017.

720 de Gouw, J. A., Gilman, J. B., Kim, S.-W., Alvarez, S. L., Dusanter, S., Graus, M.,
721 Griffith, S. M., Isaacman-VanWertz, G., Kuster, W. C., Lefer, B. L., Lerner, B. M.,
722 McDonald, B. C., Rappenglück, B., Roberts, J. M., Stevens, P. S., Stutz, J.,
723 Thalman, R., Veres, P. R., Volkamer, R., Warneke, C., Washenfelder, R. A., and
724 Young, C. J.: Chemistry of Volatile Organic Compounds in the Los Angeles Basin:
725 Formation of Oxygenated Compounds and Determination of Emission Ratios,

726   Journal of Geophysical Research: Atmospheres, 123, 2298-2319,
727   https://doi.org/10.1002/2017JD027976, 2018.
728 Dieu Hien, V. T., Lin, C., Thanh, V. C., Kim Oanh, N. T., Thanh, B. X., Weng, C.-E.,
729   Yuan, C.-S., and Rene, E. R.: An overview of the development of vertical sampling
730   technologies for ambient volatile organic compounds (VOCs), J Environ Manage,
731   247, 401-412, https://doi.org/10.1016/j.jenvman.2019.06.090, 2019.
732 Fan, M.-Y., Zhang, Y.-L., Lin, Y.-C., Li, L., Xie, F., Hu, J., Mozaffar, A., and Cao, F.:
733   Source apportionments of atmospheric volatile organic compounds in Nanjing,
734   China during high ozone pollution season, Chemosphere, 263, 128025,
735   https://doi.org/10.1016/j.chemosphere.2020.128025, 2021.
736 Fry, J. L., Brown, S. S., Middlebrook, A. M., Edwards, P. M., Campuzano-Jost, P., Day,
737   D. A., Jimenez, J. L., Allen, H. M., Ryerson, T. B., Pollack, I., Graus, M., Warneke,
738   C., de Gouw, J. A., Brock, C. A., Gilman, J., Lerner, B. M., Dubé, W. P., Liao, J.,
739   and Welti, A.: Secondary organic aerosol (SOA) yields from NO_3 radical +
740   isoprene based on nighttime aircraft power plant plume transects, Atmos. Chem.
741   Phys., 18, 11663-11682, https://doi.org/10.5194/acp-18-11663-2018, 2018.
742 Geng, F., Zhang, Q., Tie, X., Huang, M., Ma, X., Deng, Z., Yu, Q., Quan, J., and Zhao,
743   C.: Aircraft measurements of O_3, NO_x, CO, VOCs, and SO_2 in the Yangtze River
744   Delta   region,   Atmos   Environ,   43,   584-593,
745   https://doi.org/10.1016/j.atmosenv.2008.10.021, 2009.
746 Geyer, A., and Stutz, J.: Vertical profiles of NO_3, N_2O_5, O_3, and NO_x in the nocturnal
747   boundary layer: 2. Model studies on the altitude dependence of composition and
748   chemistry, Journal of Geophysical Research: Atmospheres, 109,
749   https://doi.org/10.1029/2003jd004211, 2004.
750 Gkatzelis, G. I., Coggon, M. M., McDonald, B. C., Peischl, J., Gilman, J. B., Aikin, K.
751   C., Robinson, M. A., Canonaco, F., Prevot, A. S. H., Trainer, M., and Warneke, C.:
752   Observations Confirm that Volatile Chemical Products Are a Major Source of
753   Petrochemical Emissions in U.S. Cities, Environ Sci Technol,
754   https://doi.org/10.1021/acs.est.0c05471, 2021.
755 Gómez, M. C., Durana, N., García, J. A., de Blas, M., Sáez de Cámara, E., García-Ruiz,
756   E., Gangoiti, G., Torre-Pascual, E., and Iza, J.: Long-term measurement of
757   biogenic volatile organic compounds in a rural background area: Contribution to
758   ozone   formation,   Atmos   Environ,   224,   117315,
759   https://doi.org/10.1016/j.atmosenv.2020.117315, 2020.
760 Greenberg, J. P., Guenther, A., Zimmerman, P., Baugh, W., Geron, C., Davis, K.,
761   Helmig, D., and Klinger, L. F.: Tethered balloon measurements of biogenic VOCs
762   in the atmospheric boundary layer, Atmos Environ, 33, 855-867,
763   https://doi.org/10.1016/S1352-2310(98)00302-1, 1999.
764 Guo, H., Cheng, H. R., Ling, Z. H., Louie, P. K. K., and Ayoko, G. A.: Which emission
765   sources are responsible for the volatile organic compounds in the atmosphere of
766   Pearl   River   Delta?,   J   Hazard   Mater,   188,   116-124,
767   https://doi.org/10.1016/j.jhazmat.2011.01.081, 2011.

Atmospheric
Chemistry
and Physics
Discussions

768   Hayes, P. L., Ortega, A. M., Cubison, M. J., Froyd, K. D., Zhao, Y., Cliff, S. S., Hu, W.
769   W., Toohey, D. W., Flynn, J. H., Lefer, B. L., Grossberg, N., Alvarez, S.,
770   Rappenglück, B., Taylor, J. W., Allan, J. D., Holloway, J. S., Gilman, J. B., Kuster,
771   W. C., de Gouw, J. A., Massoli, P., Zhang, X., Liu, J., Weber, R. J., Corrigan, A.
772   L., Russell, L. M., Isaacman, G., Worton, D. R., Kreisberg, N. M., Goldstein, A.
773   H., Thalman, R., Waxman, E. M., Volkamer, R., Lin, Y. H., Surratt, J. D.,
774   Kleindienst, T. E., Offenberg, J. H., Dusanter, S., Griffith, S., Stevens, P. S.,
775   Brioude, J., Angevine, W. M., and Jimenez, J. L.: Organic aerosol composition and
776   sources in Pasadena, California, during the 2010 CalNex campaign, Journal of
777   Geophysical Research: Atmospheres, 118, 9233-9257,
778   https://doi.org/10.1002/jgrd.50530, 2013.
779   He, X., Yuan, B., Wu, C., Wang, S., Wang, C., Huangfu, Y., Qi, J., Ma, N., Xu, W.,
780   Wang, M., Chen, W., Su, H., Cheng, Y., and Shao, M.: Volatile organic compounds
781   in wintertime North China Plain: Insights from measurements of proton transfer
782   reaction time-of-flight mass spectrometer (PTR-ToF-MS), Journal of
783   Environmental Sciences, https://doi.org/10.1016/j.jes.2021.08.010, 2022.
784   Hornbrook, R. S., Blake, D. R., Diskin, G. S., Fried, A., Fuelberg, H. E., Meinardi, S.,
785   Mikoviny, T., Richter, D., Sachse, G. W., Vay, S. A., Walega, J., Weibring, P.,
786   Weinheimer, A. J., Wiedinmyer, C., Wisthaler, A., Hills, A., Riemer, D. D., and
787   Apel, E. C.: Observations of nonmethane organic compounds during ARCTAS
788   − Part 1: Biomass burning emissions and plume enhancements, Atmos.
789   Chem. Phys., 11, 11103-11130, 10.5194/acp-11-11103-2011, 2011.
790   Hu, L., Millet, D. B., Kim, S. Y., Wells, K. C., Griffis, T. J., Fischer, E. V., Helmig, D.,
791   Hueber, J., and Curtis, A. J.: North American acetone sources determined from tall
792   tower measurements and inverse modeling, Atmos. Chem. Phys., 13, 3379-3392,
793   https://doi.org/10.5194/acp-13-3379-2013, 2013.
794   Hu, L., Millet, D. B., Baasandorj, M., Griffis, T. J., Travis, K. R., Tessum, C. W.,
795   Marshall, J. D., Reinhart, W. F., Mikoviny, T., Müller, M., Wisthaler, A., Graus,
796   M., Warneke, C., and de Gouw, J.: Emissions of C6–C8 aromatic compounds in
797   the United States: Constraints from tall tower and aircraft measurements, Journal
798   of Geophysical Research: Atmospheres, 120, 826-842,
799   https://doi.org/10.1002/2014JD022627, 2015a.
800   Hu, L., Millet, D. B., Baasandorj, M., Griffis, T. J., Turner, P., Helmig, D., Curtis, A. J.,
801   and Hueber, J.: Isoprene emissions and impacts over an ecological transition
802   region in the U.S. Upper Midwest inferred from tall tower measurements, Journal
803   of Geophysical Research: Atmospheres, 120, 3553-3571,
804   https://doi.org/10.1002/2014jd022732, 2015b.
805   Hu, W., Hu, M., Hu, W., Jimenez, J. L., Yuan, B., Chen, W., Wang, M., Wu, Y., Chen,
806   C., Wang, Z., Peng, J., Zeng, L., and Shao, M.: Chemical composition, sources,
807   and aging process of submicron aerosols in Beijing: Contrast between summer and
808   winter, Journal of Geophysical Research: Atmospheres, 121, 1955-1977,
809   https://doi.org/10.1002/2015JD024020, 2016.

810 Huang, X., Ding, A., Gao, J., Zheng, B., Zhou, D., Qi, X., Tang, R., Wang, J., Ren, C.,
811   Nie, W., Chi, X., Xu, Z., Chen, L., Li, Y., Che, F., Pang, N., Wang, H., Tong, D.,
812   Qin, W., Cheng, W., Liu, W., Fu, Q., Liu, B., Chai, F., Davis, S. J., Zhang, Q., and
813   He, K.: Enhanced secondary pollution offset reduction of primary emissions
814   during COVID-19 lockdown in China, National Science Review, 8,
815   https://doi.org/10.1093/nsr/nwaa137, 2020.
816 Huangfu, Y., Yuan, B., Wang, S., Wu, C., He, X., Qi, J., de Gouw, J., Warneke, C.,
817   Gilman, J. B., Wisthaler, A., Karl, T., Graus, M., Jobson, B. T., and Shao, M.:
818   Revisiting Acetonitrile as Tracer of Biomass Burning in Anthropogenic-
819   Influenced Environments, Geophys Res Lett, 48, e2020GL092322,
820   https://doi.org/10.1029/2020GL092322, 2021.
821 Jin, X., Li, Z., Wu, T., Wang, Y., Cheng, Y., Su, T., Wei, J., Ren, R., Wu, H., Li, S.,
822   Zhang, D., and Cribb, M.: The different sensitivities of aerosol optical properties
823   to particle concentration, humidity, and hygroscopicity between the surface level
824   and the upper boundary layer in Guangzhou, China, Sci Total Environ, 803,
825   150010, https://doi.org/10.1016/j.scitotenv.2021.150010, 2022.
826 Klein, F., Farren, N. J., Bozzetti, C., Daellenbach, K. R., Kilic, D., Kumar, N. K., Pieber,
827   S. M., Slowik, J. G., Tuthill, R. N., Hamilton, J. F., Baltensperger, U., Prévôt, A.
828   S. H., and El Haddad, I.: Indoor terpene emissions from cooking with herbs and
829   pepper and their secondary organic aerosol production potential, Scientific
830   Reports, 6, 36623, 10.1038/srep36623, 2016.
831 Koss, A., Yuan, B., Warneke, C., Gilman, J. B., Lerner, B. M., Veres, P. R., Peischl, J.,
832   Eilerman, S., Wild, R., Brown, S. S., Thompson, C. R., Ryerson, T., Hanisco, T.,
833   Wolfe, G. M., Clair, J. M. S., Thayer, M., Keutsch, F. N., Murphy, S., and de Gouw,
834   J.: Observations of VOC emissions and photochemical products over US oil- and
835   gas-producing regions using high-resolution H_3O+ CIMS (PTR-ToF-MS),
836   Atmospheric Measurement Techniques, 10, http://dx.doi.org/10.5194/amt-10-
837   2941-2017, 2017.
838 Li, X.-B., Wang, D., Lu, Q.-C., Peng, Z.-R., Fu, Q., Hu, X.-M., Huo, J., Xiu, G., Li, B.,
839   Li, C., Wang, D.-S., and Wang, H.: Three-dimensional analysis of ozone and $PM_{2.5}$
840   distributions obtained by observations of tethered balloon and unmanned aerial
841   vehicle in Shanghai, China, Stoch Env Res Risk A, 32, 1189-1203,
842   https://doi.org/10.1007/s00477-018-1524-2, 2018.
843 Li, X.-B., Fan, G., Lou, S., Yuan, B., Wang, X., and Shao, M.: Transport and boundary
844   layer interaction contribution to extremely high surface ozone levels in eastern
845   China, Environ Pollut, 268, 115804, https://doi.org/10.1016/j.envpol.2020.115804,
846   2021a.
847 Li, X.-B., Peng, Z.-R., Wang, D., Li, B., Huangfu, Y., Fan, G., Wang, H., and Lou, S.:
848   Vertical distributions of boundary-layer ozone and fine aerosol particles during the
849   emission control period of the G20 summit in Shanghai, China, Atmospheric
850   Pollution Research, 12, 352-364, https://doi.org/10.1016/j.apr.2020.09.016, 2021b.
851 Li, X.-B., Yuan, B., Parrish, D. D., Chen, D., Song, Y., Yang, S., Liu, Z., and Shao, M.:

852   Long-term trend of ozone in southern China reveals future mitigation strategy for
853   air pollution, Atmos Environ, 269, 118869, 10.1016/j.atmosenv.2021.118869,
854   2022.
855   Liebmann, J., Sobanski, N., Schuladen, J., Karu, E., Hellén, H., Hakola, H., Zha, Q.,
856   Ehn, M., Riva, M., Heikkinen, L., Williams, J., Fischer, H., Lelieveld, J., and
857   Crowley, J. N.: Alkyl nitrates in the boreal forest: formation via the NO_3^-, OH^- and
858   O_3-induced oxidation of biogenic volatile organic compounds and ambient
859   lifetimes, Atmos. Chem. Phys., 19, 10391-10403, https://doi.org/10.5194/acp-19-
860   10391-2019, 2019.
861   Liu, B., Liang, D., Yang, J., Dai, Q., Bi, X., Feng, Y., Yuan, J., Xiao, Z., Zhang, Y., and
862   Xu, H.: Characterization and source apportionment of volatile organic compounds
863   based on 1-year of observational data in Tianjin, China, Environ Pollut, 218, 757-
864   769, https://doi.org/10.1016/j.envpol.2016.07.072, 2016.
865   Liu, Y., Wang, H., Jing, S., Zhou, M., Lou, S., Qu, K., Qiu, W., Wang, Q., Li, S., Gao,
866   Y., Liu, Y., Li, X., Peng, Z.-R., Chen, J., and Lu, K.: Vertical Profiles of Volatile
867   Organic Compounds in Suburban Shanghai, Adv Atmos Sci, 38, 1177-1187,
868   https://doi.org/10.1007/s00376-021-0126-y, 2021.
869   Ma, Z., Zhang, X., Xu, J., Zhao, X., and Meng, W.: Characteristics of ozone vertical
870   profile observed in the boundary layer around Beijing in autumn, Journal of
871   Environmental Sciences, 23, 1316-1324, https://doi.org/10.1016/s1001-
872   0742(10)60557-8, 2011.
873   McDonald, B. C., de Gouw, J. A., Gilman, J. B., Jathar, S. H., Akherati, A., Cappa, C.
874   D., Jimenez, J. L., Lee-Taylor, J., Hayes, P. L., McKeen, S. A., Cui, Y. Y., Kim, S.-
875   W., Gentner, D. R., Isaacman-VanWertz, G., Goldstein, A. H., Harley, R. A., Frost,
876   G. J., Roberts, J. M., Ryerson, T. B., and Trainer, M.: Volatile chemical products
877   emerging as largest petrochemical source of urban organic emissions, Science, 359,
878   760, https://doi.org/10.1126/science.aaq0524, 2018.
879   Millet, D. B., Apel, E., Henze, D. K., Hill, J., Marshall, J. D., Singh, H. B., and Tessum,
880   C. W.: Natural and Anthropogenic Ethanol Sources in North America and Potential
881   Atmospheric Impacts of Ethanol Fuel Use, Environ Sci Technol, 46, 8484-8492,
882   https://doi.org/10.1021/es300162u, 2012.
883   Millet, D. B., Baasandorj, M., Hu, L., Mitroo, D., Turner, J., and Williams, B. J.:
884   Nighttime Chemistry and Morning Isoprene Can Drive Urban Ozone Downwind
885   of a Major Deciduous Forest, Environ Sci Technol, 50, 4335-4342,
886   https://doi.org/10.1021/acs.est.5b06367, 2016.
887   Mo, Z., Shao, M., and Lu, S.: Compilation of a source profile database for hydrocarbon
888   and OVOC emissions in China, Atmos Environ, 143, 209-217,
889   https://doi.org/10.1016/j.atmosenv.2016.08.025, 2016.
890   Mo, Z., Huang, S., Yuan, B., Pei, C., Song, Q., Qi, J., Wang, M., Wang, B., Wang, C.,
891   Li, M., Zhang, Q., and Shao, M.: Deriving emission fluxes of volatile organic
892   compounds from tower observation in the Pearl River Delta, China, Sci Total
893   Environ, 741, 139763, https://doi.org/10.1016/j.scitotenv.2020.139763, 2020.

894 Müller, M., Anderson, B. E., Beyersdorf, A. J., Crawford, J. H., Diskin, G. S., Eichler,
895   P., Fried, A., Keutsch, F. N., Mikoviny, T., Thornhill, K. L., Walega, J. G.,
896   Weinheimer, A. J., Yang, M., Yokelson, R. J., and Wisthaler, A.: In situ
897   measurements and modeling of reactive trace gases in a small biomass burning
898   plume, Atmos. Chem. Phys., 16, 3813-3824, 10.5194/acp-16-3813-2016, 2016.
899 Ng, N. L., Brown, S. S., Archibald, A. T., Atlas, E., Cohen, R. C., Crowley, J. N., Day,
900   D. A., Donahue, N. M., Fry, J. L., Fuchs, H., Griffin, R. J., Guzman, M. I.,
901   Herrmann, H., Hodzic, A., Iinuma, Y., Jimenez, J. L., Kiendler-Scharr, A., Lee, B.
902   H., Luecken, D. J., Mao, J. Q., McLaren, R., Mutzel, A., Osthoff, H. D., Ouyang,
903   B., Picquet-Varrault, B., Platt, U., Pye, H. O. T., Rudich, Y., Schwantes, R. H.,
904   Shiraiwa, M., Stutz, J., Thornton, J. A., Tilgner, A., Williams, B. J., and Zaveri, R.
905   A.: Nitrate radicals and biogenic volatile organic compounds: oxidation,
906   mechanisms, and organic aerosol, Atmos. Chem. Phys., 17, 2103-2162,
907   https://doi.org/10.5194/acp-17-2103-2017, 2017.
908 Pallavi, Sinha, B., and Sinha, V.: Source apportionment of volatile organic compounds
909   in the northwest Indo-Gangetic Plain using a positive matrix factorization model,
910   Atmos. Chem. Phys., 19, 15467-15482, https://doi.org/10.5194/acp-19-15467-
911   2019, 2019.
912 Pernov, J. B., Bossi, R., Lebourgeois, T., Nøjgaard, J. K., Holzinger, R., Hjorth, J. L.,
913   and Skov, H.: Atmospheric VOC measurements at a High Arctic site:
914   characteristics and source apportionment, Atmos. Chem. Phys., 21, 2895-2916,
915   https://doi.org/10.5194/acp-21-2895-2021, 2021.
916 Qi, J., Mo, Z., Yuan, B., Huang, S., Huangfu, Y., Wang, Z., Li, X., Yang, S., Wang, W.,
917   Zhao, Y., Wang, X., Wang, W., Liu, K., and Shao, M.: An observation approach in
918   evaluation of ozone production to precursor changes during the COVID-19
919   lockdown, Atmos Environ, 262, 118618,
920   https://doi.org/10.1016/j.atmosenv.2021.118618, 2021.
921 Qin, J., Wang, X., Yang, Y., Qin, Y., Shi, S., Xu, P., Chen, R., Zhou, X., Tan, J., and
922   Wang, X.: Source apportionment of VOCs in a typical medium-sized city in North
923   China Plain and implications on control policy, Journal of Environmental Sciences,
924   107, 26-37, https://doi.org/10.1016/j.jes.2020.10.005, 2021.
925 Sangiorgi, G., Ferrero, L., Perrone, M. G., Bolzacchini, E., Duane, M., and Larsen, B.
926   R.: Vertical distribution of hydrocarbons in the low troposphere below and above
927   the mixing height: Tethered balloon measurements in Milan, Italy, Environ Pollut,
928   159, 3545-3552, https://doi.org/10.1016/j.envpol.2011.08.012, 2011.
929 Squires, F. A., Nemitz, E., Langford, B., Wild, O., Drysdale, W. S., Acton, W. J. F., Fu,
930   P., Grimmond, C. S. B., Hamilton, J. F., Hewitt, C. N., Hollaway, M., Kotthaus, S.,
931   Lee, J., Metzger, S., Pingintha-Durden, N., Shaw, M., Vaughan, A. R., Wang, X.,
932   Wu, R., Zhang, Q., and Zhang, Y.: Measurements of traffic-dominated pollutant
933   emissions in a Chinese megacity, Atmos. Chem. Phys., 20, 8737-8761,
934   https://doi.org/10.5194/acp-20-8737-2020, 2020.
935 Stutz, J., Alicke, B., Ackermann, R., Geyer, A., White, A., and Williams, E.: Vertical

936   profiles of NO_3, N_2O_5, O_3, and NO_x in the nocturnal boundary layer: 1.
937   Observations during the Texas Air Quality Study 2000, Journal of Geophysical
938   Research: Atmospheres, 109, https://doi.org/10.1029/2003jd004209, 2004.
939 Tan, Y., Han, S., Chen, Y., Zhang, Z., Li, H., Li, W., Yuan, Q., Li, X., Wang, T., and Lee,
940   S.-c.: Characteristics and source apportionment of volatile organic compounds
941   (VOCs) at a coastal site in Hong Kong, Sci Total Environ, 777, 146241,
942   https://doi.org/10.1016/j.scitotenv.2021.146241, 2021.
943 Ting, M., Yue-si, W., Jie, J., Fang-kun, W., and Mingxing, W.: The vertical distributions
944   of VOCs in the atmosphere of Beijing in autumn, Sci Total Environ, 390, 97-108,
945   https://doi.org/10.1016/j.scitotenv.2007.08.035, 2008.
946 Udina, M., Soler, M. R., Olid, M., Jiménez-Esteve, B., and Bech, J.: Pollutant vertical
947   mixing in the nocturnal boundary layer enhanced by density currents and low-level
948   jets: two representative case studies, Bound-lay Meteorol, 174, 203-230,
949   https://doi.org/10.1007/s10546-019-00483-y, 2020.
950 Ulbrich, I. M., Canagaratna, M. R., Zhang, Q., Worsnop, D. R., and Jimenez, J. L.:
951   Interpretation of organic components from Positive Matrix Factorization of
952   aerosol mass spectrometric data, Atmos. Chem. Phys., 9, 2891-2918,
953   https://doi.org/10.5194/acp-9-2891-2009, 2009.
954 Velasco, E., Marquez, C., Bueno, E., Bernabe, R. M., Sanchez, A., Fentanes, O.,
955   Wohrnschimmel, H., Cardenas, B., Kamilla, A., Wakamatsu, S., and Molina, L. T.:
956   Vertical distribution of ozone and VOCs in the low boundary layer of Mexico City,
957   Atmos. Chem. Phys., 8, 3061-3079, https://doi.org/10.5194/acp-8-3061-2008,
958   2008.
959 Veres, P. R., Faber, P., Drewnick, F., Lelieveld, J., and Williams, J.: Anthropogenic
960   sources of VOC in a football stadium: Assessing human emissions in the
961   atmosphere, Atmos Environ, 77, 1052-1059,
962   https://doi.org/10.1016/j.atmosenv.2013.05.076, 2013.
963 Vo, T.-D.-H., Lin, C., Weng, C.-E., Yuan, C.-S., Lee, C.-W., Hung, C.-H., Bui, X.-T.,
964   Lo, K.-C., and Lin, J.-X.: Vertical stratification of volatile organic compounds and
965   their photochemical product formation potential in an industrial urban area, J
966   Environ Manage, 217, 327-336, https://doi.org/10.1016/j.jenvman.2018.03.101,
967   2018.
968 Wang, C., Yuan, B., Wu, C., Wang, S., Qi, J., Wang, B., Wang, Z., Hu, W., Chen, W.,
969   Ye, C., Wang, W., Sun, Y., Wang, C., Huang, S., Song, W., Wang, X., Yang, S.,
970   Zhang, S., Xu, W., Ma, N., Zhang, Z., Jiang, B., Su, H., Cheng, Y., Wang, X., and
971   Shao, M.: Measurements of higher alkanes using NO+ chemical ionization in
972   PTR-ToF-MS: important contributions of higher alkanes to secondary organic
973   aerosols in China, Atmos. Chem. Phys., 20, 14123-14138,
974   https://doi.org/10.5194/acp-20-14123-2020, 2020a.
975 Wang, T., Xue, L., Brimblecombe, P., Lam, Y. F., Li, L., and Zhang, L.: Ozone pollution
976   in China: A review of concentrations, meteorological influences, chemical
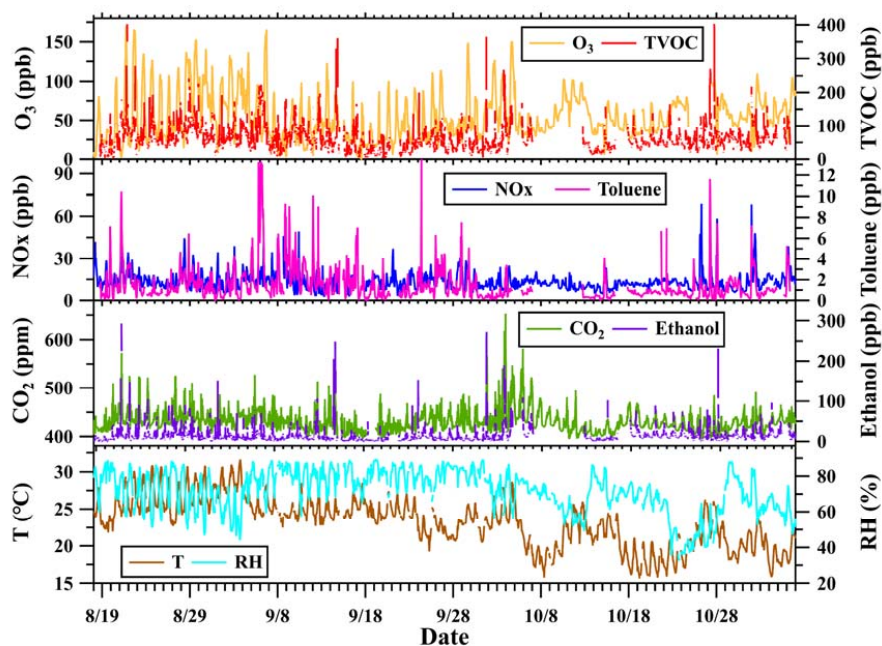977   precursors, and effects, Sci Total Environ, 575, 1582-1596,

978   https://doi.org/10.1016/j.scitotenv.2016.10.081, 2017.
979 Wang, Y., Wang, Y., Tang, G., Yang, Y., Li, X., Yao, D., Wu, S., Kang, Y., Wang, M.,
980   and Wang, Y.: High gaseous carbonyl concentrations in the upper boundary layer
981   in   Shijiazhuang,   China,   Sci   Total   Environ,   799,   149438,
982   https://doi.org/10.1016/j.scitotenv.2021.149438, 2021.
983 Wang, Y. H., Gao, W. K., Wang, S., Song, T., Gong, Z. Y., Ji, D. S., Wang, L. L., Liu,
984   Z. R., Tang, G. Q., Huo, Y. F., Tian, S. L., Li, J. Y., Li, M. G., Yang, Y., Chu, B.
985   W., Petaja, T., Kerminen, V. M., He, H., Hao, J. M., Kulmala, M., Wang, Y. S., and
986   Zhang, Y. H.: Contrasting trends of PM$_{2.5}$ and surface-ozone concentrations in
987   China   from   2013   to   2017,   National   Science   Review,   7,   1331-1339,
988   https://doi.org/10.1093/nsr/nwaa032, 2020b.
989 Wang, Z., Yuan, B., Ye, C., Roberts, J., Wisthaler, A., Lin, Y., Li, T., Wu, C., Peng, Y.,
990   Wang, C., Wang, S., Yang, S., Wang, B., Qi, J., Wang, C., Song, W., Hu, W., Wang,
991   X., Xu, W., Ma, N., Kuang, Y., Tao, J., Zhang, Z., Su, H., Cheng, Y., Wang, X.,
992   and Shao, M.: High Concentrations of Atmospheric Isocyanic Acid (HNCO)
993   Produced from Secondary Sources in China, Environ Sci Technol, 54, 11818-
994   11826, https://doi.org/10.1021/acs.est.0c02843, 2020c.
995 Warneke, C., de Gouw, J. A., Goldan, P. D., Kuster, W. C., Williams, E. J., Lerner, B.
996   M., Jakoubek, R., Brown, S. S., Stark, H., Aldener, M., Ravishankara, A. R.,
997   Roberts, J. M., Marchewka, M., Bertman, S., Sueper, D. T., McKeen, S. A.,
998   Meagher, J. F., and Fehsenfeld, F. C.: Comparison of daytime and nighttime
999   oxidation of biogenic and anthropogenic VOCs along the New England coast in
1000   summer during New England Air Quality Study 2002, Journal of Geophysical
1001   Research: Atmospheres, 109, https://doi.org/10.1029/2003jd004424, 2004.
1002 Wu, C., Wang, C., Wang, S., Wang, W., Yuan, B., Qi, J., Wang, B., Wang, H., Wang, C.,
1003   Song, W., Wang, X., Hu, W., Lou, S., Ye, C., Peng, Y., Wang, Z., Huangfu, Y., Xie,
1004   Y., Zhu, M., Zheng, J., Wang, X., Jiang, B., Zhang, Z., and Shao, M.: Measurement
1005   report: Important contributions of oxygenated compounds to emissions and
1006   chemistry of volatile organic compounds in urban air, Atmos. Chem. Phys., 20,
1007   14769-14785, https://doi.org/10.5194/acp-20-14769-2020, 2020a.
1008 Wu, F., Yu, Y., Sun, J., Zhang, J., Wang, J., Tang, G., and Wang, Y.: Characteristics,
1009   source apportionment and reactivity of ambient volatile organic compounds at
1010   Dinghu Mountain in Guangdong Province, China, Sci Total Environ, 548-549,
1011   347-359, https://doi.org/10.1016/j.scitotenv.2015.11.069, 2016.
1012 Wu, S., Tang, G., Wang, Y., Yang, Y., Yao, D., Zhao, W., Gao, W., Sun, J., and Wang,
1013   Y.: Vertically decreased VOC concentration and reactivity in the planetary
1014   boundary layer in winter over the North China Plain, Atmos Res, 240, 104930,
1015   https://doi.org/10.1016/j.atmosres.2020.104930, 2020b.
1016 Wu, S., Tang, G. Q., Wang, Y. H., Mai, R., Yao, D., Kang, Y. Y., Wang, Q. L., and Wang,
1017   Y. S.: Vertical Evolution of Boundary Layer Volatile Organic Compounds in
1018   Summer over the North China Plain and the Differences with Winter, Adv Atmos
1019   Sci, 38, 1165-1176, https://doi.org/10.1007/s00376-020-0254-9, 2021.

Xia, S.-Y., Wang, C., Zhu, B., Chen, X., Feng, N., Yu, G.-H., and Huang, X.-F.: Long-term observations of oxygenated volatile organic compounds (OVOCs) in an urban atmosphere in southern China, 2014–2019, Environ Pollut, 270, 116301, https://doi.org/10.1016/j.envpol.2020.116301, 2021.

Xue, L., Wang, T., Simpson, I. J., Ding, A., Gao, J., Blake, D. R., Wang, X., Wang, W., Lei, H., and Jin, D.: Vertical distributions of non-methane hydrocarbons and halocarbons in the lower troposphere over northeast China, Atmos Environ, 45, 6501-6509, https://doi.org/10.1016/j.atmosenv.2011.08.072, 2011.

Yan, F., Chen, W., Jia, S., Zhong, B., Yang, L., Mao, J., Chang, M., Shao, M., Yuan, B., Situ, S., Wang, X., Chen, D., and Wang, X.: Stabilization for the secondary species contribution to $PM_{2.5}$ in the Pearl River Delta (PRD) over the past decade, China: A meta-analysis, Atmos Environ, 242, 117817, https://doi.org/10.1016/j.atmosenv.2020.117817, 2020.

Ye, C., Yuan, B., Lin, Y., Wang, Z., Hu, W., Li, T., Chen, W., Wu, C., Wang, C., Huang, S., Qi, J., Wang, B., Wang, C., Song, W., Wang, X., Zheng, E., Krechmer, J. E., Ye, P., Zhang, Z., Wang, X., Worsnop, D. R., and Shao, M.: Chemical characterization of oxygenated organic compounds in the gas phase and particle phase using iodide CIMS with FIGAERO in urban air, Atmos. Chem. Phys., 21, 8455-8478, https://doi.org/10.5194/acp-21-8455-2021, 2021.

Yuan, B., Shao, M., de Gouw, J., Parrish, D. D., Lu, S., Wang, M., Zeng, L., Zhang, Q., Song, Y., Zhang, J., and Hu, M.: Volatile organic compounds (VOCs) in urban air: How chemistry affects the interpretation of positive matrix factorization (PMF) analysis, Journal of Geophysical Research: Atmospheres, 117, https://doi.org/10.1029/2012jd018236, 2012.

Yuan, B., Koss, A., Warneke, C., Gilman, J. B., Lerner, B. M., Stark, H., and de Gouw, J. A.: A high-resolution time-of-flight chemical ionization mass spectrometer utilizing hydronium ions (H_3O+ ToF-CIMS) for measurements of volatile organic compounds in the atmosphere, Atmospheric Measurement Techniques, 9, 2735-2752, https://doi.org/10.5194/amt-9-2735-2016, 2016.

Yuan, B., Koss, A. R., Warneke, C., Coggon, M., Sekimoto, K., and de Gouw, J. A.: Proton-Transfer-Reaction Mass Spectrometry: Applications in Atmospheric Sciences, Chem Rev, 117, 13187-13229, https://doi.org/10.1021/acs.chemrev.7b00325, 2017.

Yuan, Z., Zhong, L., Lau, A. K. H., Yu, J. Z., and Louie, P. K. K.: Volatile organic compounds in the Pearl River Delta: Identification of source regions and recommendations for emission-oriented monitoring strategies, Atmos Environ, 76, 162-172, https://doi.org/10.1016/j.atmosenv.2012.11.034, 2013.

Zhang, H., Zhang, Y., Huang, Z., Acton, W. J. F., Wang, Z., Nemitz, E., Langford, B., Mullinger, N., Davison, B., Shi, Z., Liu, D., Song, W., Yang, W., Zeng, J., Wu, Z., Fu, P., Zhang, Q., and Wang, X.: Vertical profiles of biogenic volatile organic compounds as observed online at a tower in Beijing, J Environ Sci (China), 95, 33-42, https://doi.org/10.1016/j.jes.2020.03.032, 2020.

1062 Zhang, K., Xiu, G., Zhou, L., Bian, Q., Duan, Y., Fei, D., Wang, D., and Fu, Q.: Vertical
1063   distribution of volatile organic compounds within the lower troposphere in late
1064   spring of Shanghai, Atmos Environ, 186, 150-157,
1065   https://doi.org/10.1016/j.atmosenv.2018.03.044, 2018.
1066 Zhang, K., Zhou, L., Fu, Q., Yan, L., Bian, Q., Wang, D., and Xiu, G.: Vertical
1067   distribution of ozone over Shanghai during late spring: A balloon-borne
1068   observation, Atmos Environ, 208, 48-60,
1069   https://doi.org/10.1016/j.atmosenv.2019.03.011, 2019.
1070 Zhang, Y., Wang, X., Barletta, B., Simpson, I. J., Blake, D. R., Fu, X., Zhang, Z., He,
1071   Q., Liu, T., Zhao, X., and Ding, X.: Source attributions of hazardous aromatic
1072   hydrocarbons in urban, suburban and rural areas in the Pearl River Delta (PRD)
1073   region, J Hazard Mater, 250-251, 403-411,
1074   https://doi.org/10.1016/j.jhazmat.2013.02.023, 2013.
1075 Zhao, D., Pullinen, I., Fuchs, H., Schrade, S., Wu, R., Acir, I. H., Tillmann, R., Rohrer,
1076   F., Wildt, J., Guo, Y., Kiendler-Scharr, A., Wahner, A., Kang, S., Vereecken, L.,
1077   and Mentel, T. F.: Highly oxygenated organic molecule (HOM) formation in the
1078   isoprene oxidation by NO_3 radical, Atmos. Chem. Phys., 21, 9681-9704,
1079   https://doi.org/10.5194/acp-21-9681-2021, 2021.
1080 Zheng, J., Yu, Y., Mo, Z., Zhang, Z., Wang, X., Yin, S., Peng, K., Yang, Y., Feng, X.,
1081   and Cai, H.: Industrial sector-based volatile organic compound (VOC) source
1082   profiles measured in manufacturing facilities in the Pearl River Delta, China, Sci
1083   Total Environ, 456-457, 127-136, https://doi.org/10.1016/j.scitotenv.2013.03.055,
1084   2013.
1085 Zhou, X., Li, Z., Zhang, T., Wang, F., Wang, F., Tao, Y., Zhang, X., Wang, F., and Huang,
1086   J.: Volatile organic compounds in a typical petrochemical industrialized valley city
1087   of northwest China based on high-resolution PTR-MS measurements:
1088   Characterization, sources and chemical effects, Sci Total Environ, 671, 883-896,
1089   https://doi.org/10.1016/j.scitotenv.2019.03.283, 2019.
1090 Zhu, B., Han, Y., Wang, C., Huang, X., Xia, S., Niu, Y., Yin, Z., and He, L.:
1091   Understanding primary and secondary sources of ambient oxygenated volatile
1092   organic compounds in Shenzhen utilizing photochemical age-based
1093   parameterization method, Journal of Environmental Sciences, 75, 105-114,
1094   https://doi.org/10.1016/j.jes.2018.03.008, 2019.

1095

Atmospheric
Chemistry
and Physics
Discussions

Open Access

EGU

Figure 1. Time series of concentrations of some typical chemical species along with meteorological parameters during the CTT campaign. Temperature (T), relative humidity (RH), concentrations of ozone and NOx were measured at 488 m. Concentrations of VOCs, ethanol, and CO_2 were measured at 450 m.
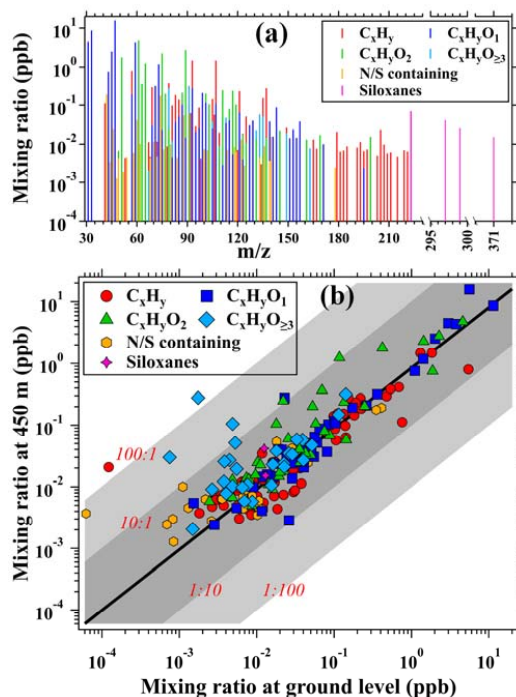
1101

Figure 2. (a) Average mass spectra of VOCs (including 225 species) obtained by PTR-

ToF-MS during the CTT campaign. (b) Scatter plots of the average VOC mixing ratios

at 450 m during the CTT campaign versus those measured at the ground level during

the GIG campaign; The black solid line indicates the ratio of 1:1; The dark grey shaded

areas indicate the ratios of 10:1 and 1:10; The light grey shaded areas indicate the ratios

of 100:1 and 1:100. C_xH_y refers to hydrocarbons. $C_xH_yO_1$ refers to VOC species

containing one oxygen atom. $C_xH_yO_2$ refers to VOC species containing two oxygen

atoms. $C_xH_yO_{\geq 3}$ refers to VOC species containing more than three oxygen atoms. N/S

containing refers to VOC species containing nitrogen or sulfur atoms.
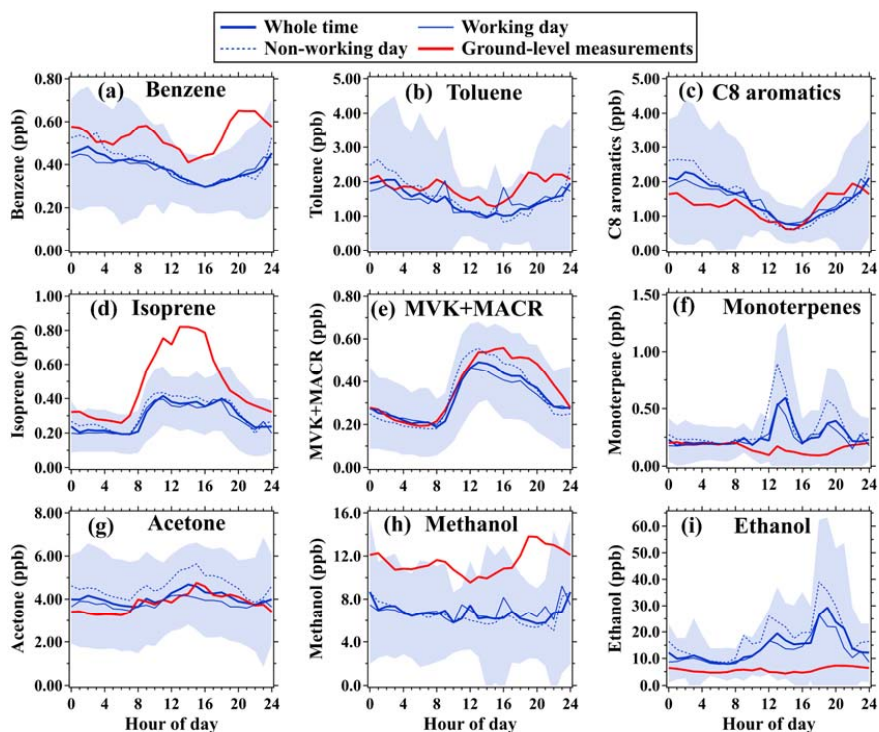
Figure 3. Diurnal variations in mixing ratios of selected VOC species measured by PTR-ToF-MS. Thick blue solid lines and shaded areas represent averages and standard deviations, respectively, during the CTT campaign (August 18–November 05, 2020). Red solid lines represent averages during the GIG campaign (September 11–November 19, 2018). Thin blue solid and dashed lines represent averages in working days and non-working (including weekends and public holidays) days, respectively, during the CTT campaign.
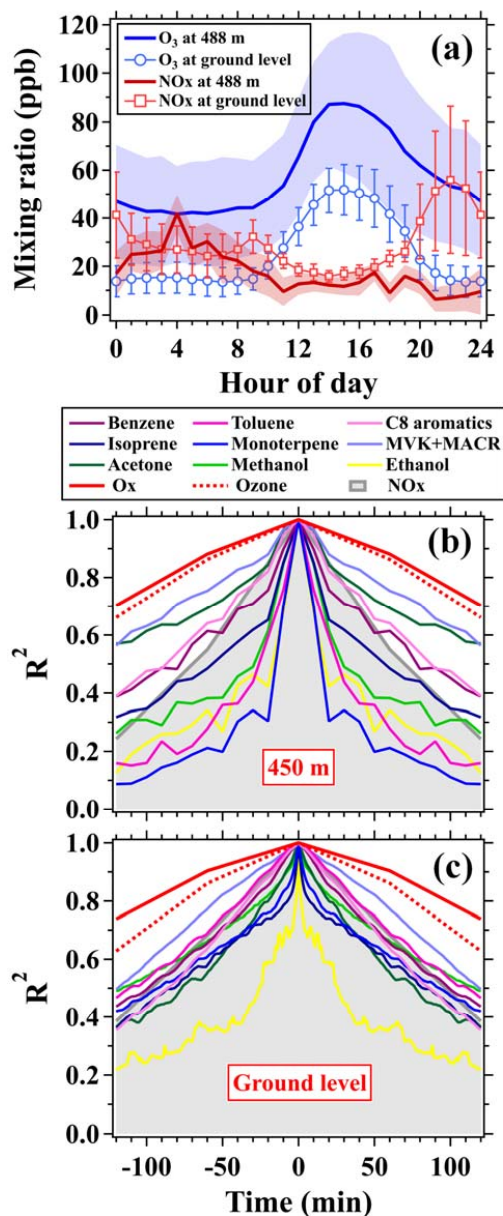
Figure 4. (a) Diurnal profiles of ozone and NOx mixing ratios measured at the 488-m site (mean ± standard deviation) and the surface site (mean ± 0.5 standard deviation) on the CTT. (b) Autocorrelation of the time series of ozone (488 m), NOx (488 m), Ox (488 m), and selected VOC species (450 m) during the CTT campaign. (c) Autocorrelation of the time series of the selected VOC species at the ground level

1125   during the GIG campaign; Autocorrelation of the time series of ozone, NOx, and Ox in

1126   panel (c) are calculated using the measurements made at the surface site of Canton

1127   Tower during the CTT campaign.

Atmospheric
Chemistry
and Physics
Discussions

Open Access

EGU
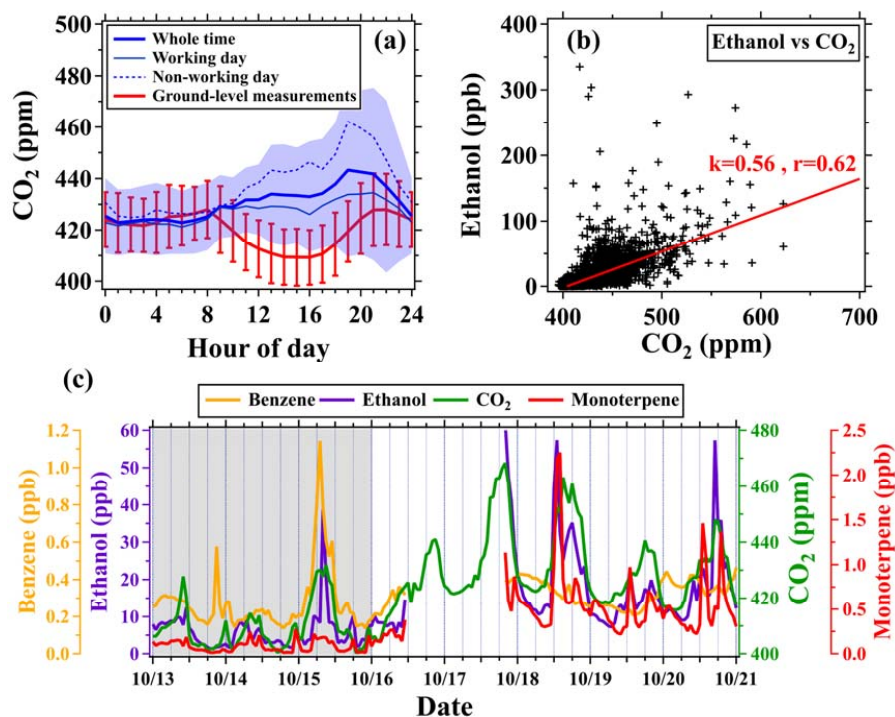
1128

Figure 5. (a) Diurnal variations in CO_2 mixing ratios at 450 m and the ground level,
respectively. (b) Scatterplots of ethanol versus CO_2 mixing ratios measured at 450 m
during the CTT campaign; The ground-level CO_2 measurements were made in the GIG
campaign. (c) Time series of benzene, ethanol, CO_2, and monoterpene mixing ratios
measured at 450 m from October 13 to 21; The grey shaded area indicates the period
(October 13–21) when the 450-m platform was closed due to the influence of Typhoon
Kompasu.
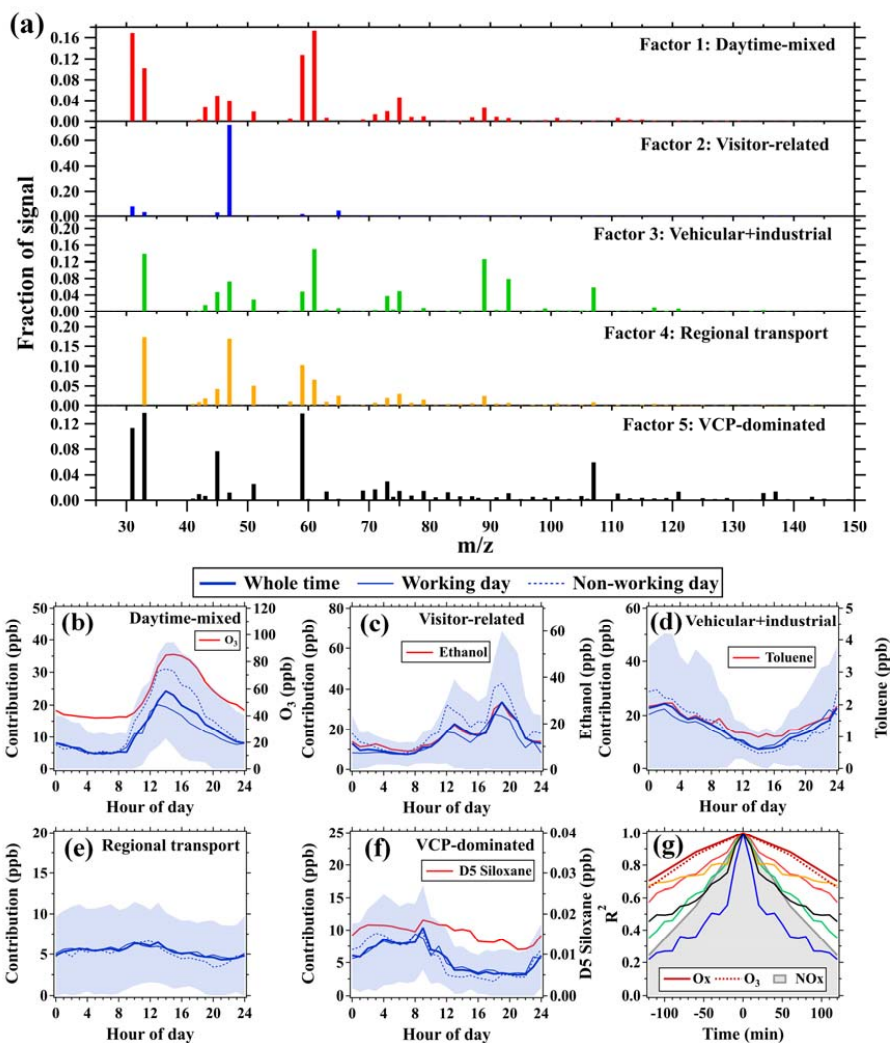
1136

Figure 6. (a) Factor profiles (m/z ⩽ 150) of the five PMF factors; Factor profiles with

a full range of the mass spectra are provided in Figure S5. (b-f) Average diurnal profiles

of the five PMF factors and source tracers. (g) Autocorrelation of the time series of the

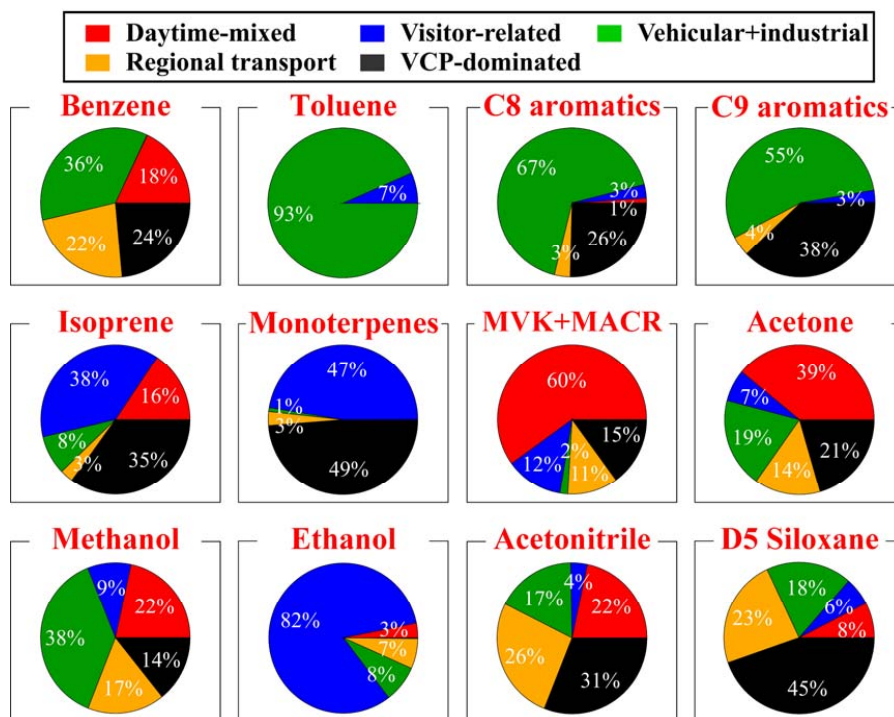five PMF factors along with Ox, ozone, and NOx mixing ratios at 488 m.
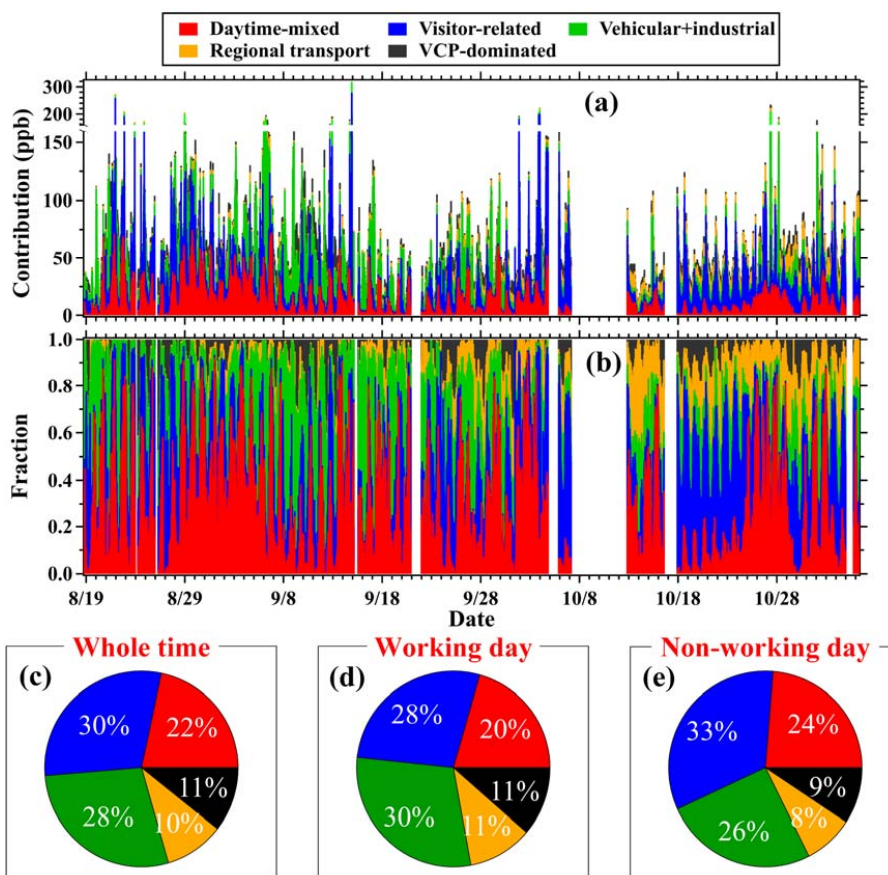
Figure 7. (a-b) Stacked time series of factor fractions and factor contributions for the
PMF analysis; (c-e) Average contributions of the five PMF factors in the whole time,
working days, and non-working days.

1145

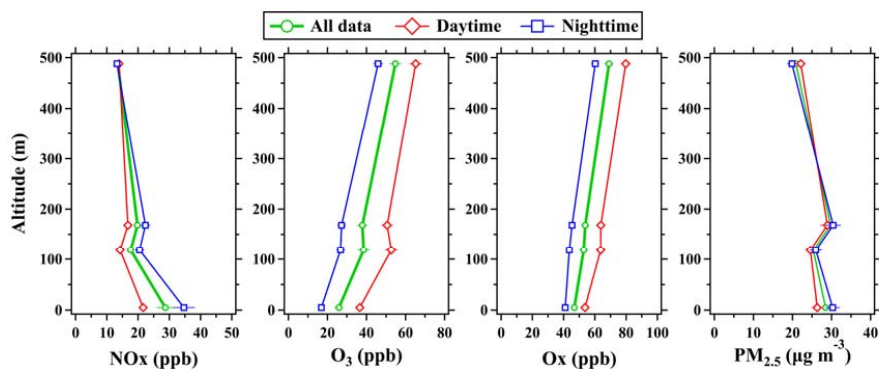**Figure 8.** (a) Average contributions of the five PMF factors to the 9 selected VOC
species during the CTT campaign.
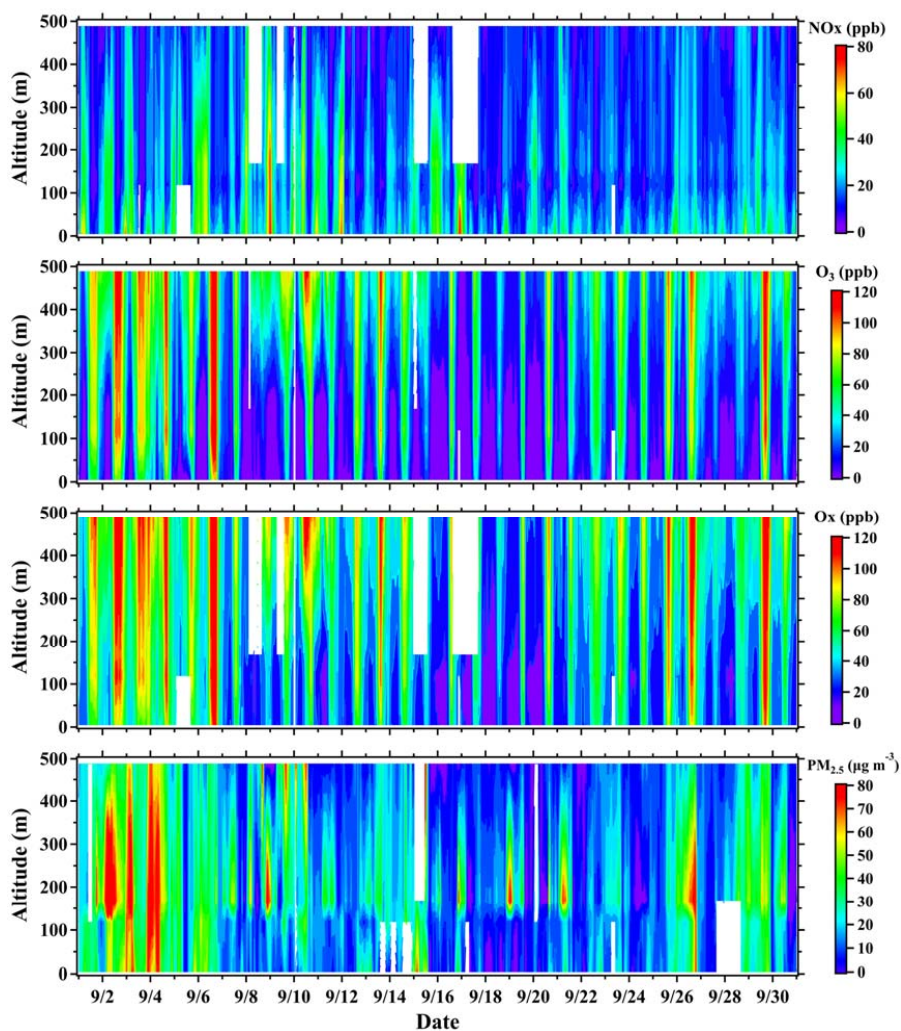
**Figure 9.** Time series of vertical profiles for O_3, NOx, Ox (O_3+NO_2), and PM2.5 concentrations in September during the CTT campaign. The contour plots are made using the measurements from the four CTT sites (5 m, 118 m, 168 m, and 488 m).

Figure 10. Average vertical profiles of O_3, NOx, Ox (O_3+NO_2), and $PM_{2.5}$ concentrations (mean ± 0.1 standard deviations) measured at the four CTT sites (5 m, 118 m, 168 m, 488 m) during the campaign. Daytime refers to the time between LT 08:00–18:00; nighttime refers to the time between LT 19:00–05:00.
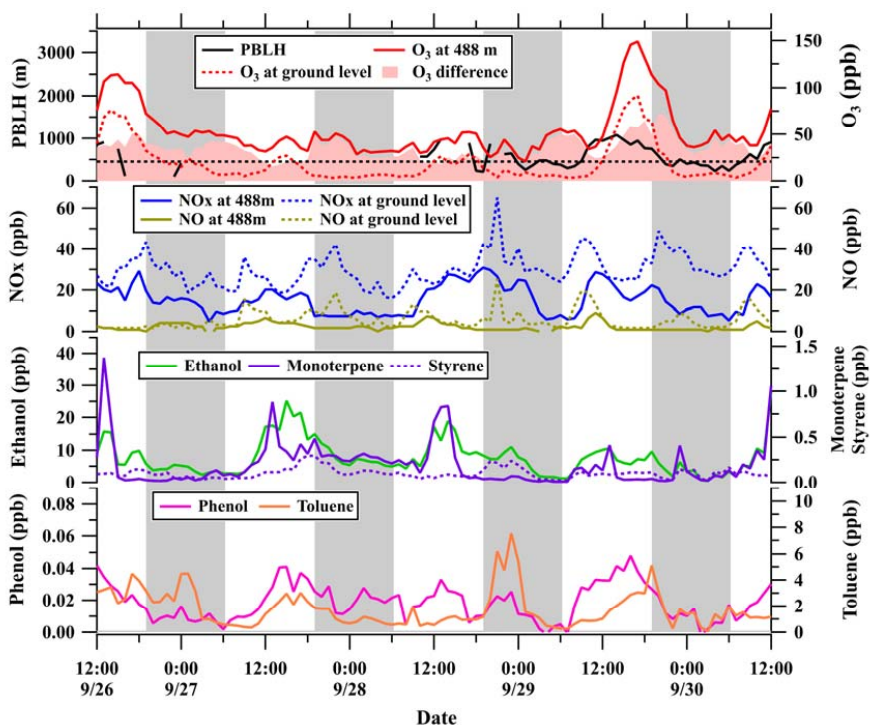
Figure 11. Time series of O_3, NOx, NO, ethanol, monoterpene, styrene, phenol, and toluene mixing ratios along with planetary boundary layer height (PBLH) during September 26–30. O_3 difference refers to the differences in ozone mixing ratios between 488 m and 5 m. Grey shaded areas indicate nighttime periods (LT 19:00–05:00).